Tribology International 193 (2024) 109356

Contents lists available at ScienceDirect

Tribology International

journal homepage: www.elsevier.com/locate/triboint

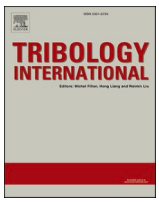

Tribological performance of 3D printed neat and carbon fiber reinforced PEEK composites

Nayan Dhakal [a,b,*], Cayetano Espejo [b], Ardian Morina [b], Nazanin Emami [a,**]

[a] Polymer-tribology group, Division of Machine Elements, Luleå University of Technology, SE 97187 Luleå, Sweden
[b] Institute of Functional Surfaces, School of Mechanical Engineering, University of Leeds, LS2 9JT Leeds, United Kingdom

ARTICLE INFO

Keywords:
3D printing
Tribology
Polymer composites
PEEK
Friction and wear
Dry sliding
Water lubrication

ABSTRACT

This work investigates the tribological behavior of neat and carbon fiber-reinforced polyether-ether-ketone (PEEK) materials processed using the fused filament fabrication (FFF) technique. The reciprocating sliding behavior of printed polymers against stainless steel (SS) under dry and water-lubricated conditions was studied. The running-in behavior and evolution of friction were dependent on the material combination and sliding conditions. PEEK reinforced with 10 wt% carbon fibers was optimal considering tribological performance. Neat PEEK exhibited a combination of abrasive and adhesive wear mechanisms, while composites primarily showed fiber-matrix debonding and delamination during sliding. The outcome of this work has significance in improving the processing design of PEEK-based materials in extrusion-based 3D printing for tribological applications.

1. Introduction

Additive manufacturing (AM) or three-dimensional (3D) printing of polymer-based materials has seen significant advancements in recent years. Fused filament fabrication (FFF) is the commonly adopted material-extrusion-based technique applicable to the processing of polymers. In general, FFF 3D printing of high-performance thermoplastics is quite challenging due to the requirement of high thermal processing conditions and complex process-structure-property relationships [1,2]. Recently, technological innovations in the AM realm have allowed the exploration of processing high-temperature thermoplastics, such as polyether-ether-ketone (PEEK), polyether-ketone-ketone (PEKK), polyetherimide (PEI), polyphenylene-sulfide (PPS), and polysulfone (PSU) [3,4]. Among others, PEEK-based materials acquired ample attention due to their widespread use in the aerospace, automotive, energy, chemical, and medical industries [4,5].

PEEK is a semicrystalline thermoplastic polymer offering excellent mechanical properties, high thermal stability, good wear resistance, and corrosion resistance making it an ideal choice in demanding applications [5]. PEEK-based materials for commercial use are mostly produced by conventional manufacturing (CM) techniques. The versatility and flexibility of PEEK allow its processing through several methods such as extrusion, injection molding, and compression molding followed by machining. CM of PEEK is known to produce high-temperature resistant parts with good anti-wear properties but usually exhibit high coefficients of friction (COF). On the other hand, the addition of solid lubricants, micro-fillers, and nanoparticles in the PEEK matrix is reported to significantly reduce the friction coefficients and further enhance the wear resistance for load-bearing applications [6,7]. Carbonaceous reinforcing fillers such as carbon fibers (CF), carbon nanotubes (CNT), and graphene derivatives have exhibited substantial improvement in the tribological performance of PEEK [8–11].

In the context of global sustainability, traditional subtractive methods are often associated with negative environmental impacts due to their prolonged production cycles and lead time which are highly energy- and resource-intensive [12]. AM offers the possibility of sustainable processing solutions with economic and environmental benefits [13]. Also, AM increases design flexibility allowing the production of complex parts resulting in reduced material wastage and production costs [14]. Furthermore, FFF technique pushes forward the limits of high-performance material fabrication towards a fast and cost-effective route with efficient workability. Despite the challenges, researchers have explored improving the processability and properties of FFF printed PEEK during the last few years. The influence of processing conditions on the characteristics, performances, and quality of FFF printed PEEK is widely investigated [1,15,16]. As a result, significant

* Corresponding author at: Polymer-tribology group, Division of Machine Elements, Luleå University of Technology, SE 97187 Luleå, Sweden.
** Corresponding author.
E-mail addresses: nayan.dhakal@ltu.se (N. Dhakal), nazanin.emami@ltu.se (N. Emami).

https://doi.org/10.1016/j.triboint.2024.109356
Received 4 July 2023; Received in revised form 24 January 2024; Accepted 29 January 2024
Available online 3 February 2024

Table 1
– Fused Filament Fabrication (FFF) printing parameters.

Process parameters	Values
Raster angle [deg]	+ 45°/− 45°
Printing speed [mm/s]	50 mm/s
Printing nozzle temperature [°C]	440
Build platform temperature [°C]	140
Chamber temperature [°C]	120
Extruder nozzle diameter [mm]	0.40 mm
Layer thickness [mm]	0.10 mm
Infill pattern	Rectilinear
Infill density [%]	100%

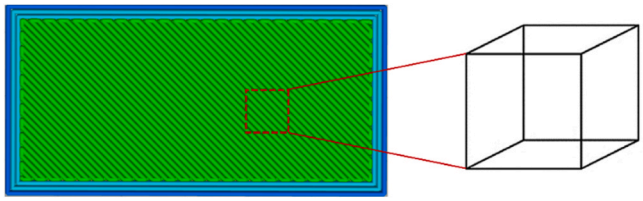

Fig. 1. Schematic representation of FFF printed block and tribological testing pin (4×4×4 mm^3).

advancements have been achieved in the improvement of mechanical properties and interlayer bonding during the printing of PEEK-based [15, 17–19] materials. However, there is a very limited report on the tribological performance of FFF printed PEEK-based materials for bearing applications [20–23].

Recently, Wang *et al.* [22] proposed a new design method with FFF 3D printing for multi-material gradient structures of carbon fiber-reinforced PEEK composites to improve tribological performance. According to Arif *et al.* [21], carbon-based fillers in FFF 3D printing of PEEK significantly reduce the friction coefficients and enhance the multi-functionality. In another study, He *et al.* [23] studied the effect of printing orientation on the tribological properties of FFF printed PEEK. Wear assessment in this study showed that printing PEEK in 45° orientation yielded relatively lower wear rates and a uniform transfer film formation. With a limited number of studies, a notable lack of information on the tribological performance of 3D printed PEEK is evident in the existing literature. For that reason, there is a need for a thorough investigation of the possibility of 3D printing PEEK and its composites for low-friction and anti-wear properties.

Therefore, this study investigates the tribological performance of in-house 3D printed PEEK-based materials for different sliding conditions. Neat and carbon fiber-filled PEEK parts were processed using material extrusion-based 3D printing to understand the evolution of friction and wear behavior of printed parts under dry sliding and water-lubricated conditions. The influence of carbon fiber reinforcement on wear mechanisms and the variation of surface topography of printed polymers arising from the sliding were analyzed. It is expected that the outcome of the presented research work will provide a better understanding of the impact of manufacturing methods on tribological performance, acting as a guide for the design of PEEK-based materials with extrusion-based additive manufacturing for tribological applications.

2. Experimental details

2.1. Materials and sample preparation

PEEK-based starting filaments with a diameter of 1.75 mm and varying contents of chopped carbon fibers (0, 10, and 20 wt%) were procured from 3DXTech Additive Manufacturing (Michigan, USA). Neat PEEK and carbon fiber-filled PEEK were chosen to study the influence of carbon fiber reinforcement on friction and wear of 3D printed parts. As specified by the supplier, the filaments were formulated using Victrex™ PEEK resins and randomly oriented carbon fibers of 5–10 μm diameter.

3D CAD models of the specimens were prepared using Autodesk Fusion 360 (California, USA). Simplify3D V5 (Cincinnati, USA) was used for layer slicing to create a printable G-code file. The G-code files were exported to the CreatBot PEEK-300 high-temperature printer (Henan Suwei, China) to additively manufacture the testing specimens using the filament wires. The filaments were pre-dried at 120°C for 12 h in an air-circulated oven before printing. The process parameters used for final printing are listed in Table 1. The polymer pins used for tribological testing (4×4×4 mm^3) were carefully cut from a 3D printed block. The as-printed top surfaces were used as the contact face against stainless steel (SS) without any surface modification. The schematic representation of FFF printed tribological testing specimen is presented in Fig. 1. Injection molded neat PEEK (450 G™) provided by Victrex™ (Lancashire, UK) was used as a reference material to compare the tribological results of 3D printed PEEK.

2.2. Density and porosity

The immersion method according to ASTM D792 [24] was used to record the apparent densities of 3D printed polymers. Distilled water was used to completely immerse the specimen during wet mass measurements. The density of water was taken as 997.8 kg/m^3 at 22°C. The volumetric porosity or void content (V) was determined based on ASTM D2734 [25] using Eq. (1).

$$V = 100(T_d - M_d)/T_d \tag{1}$$

In this equation, T_d is theoretical density (kg/m^3), and M_d is measured density (kg/m^3). The average of 3 repeated measurements is reported.

The theoretical density of the semi-crystalline PEEK was calculated based on its degree of crystallinity (X_c) using Eq. (2).

$$T_{d,semi-crystalline} = T_{d,100\%am}\left(1 - \frac{X_c}{100}\right) + T_{d,100\%cr} * \frac{X_c}{100} \tag{2}$$

In this equation, $T_{d,100\%am}$ and $T_{d,100\%cr}$ are the theoretical densities of a fully amorphous PEEK (1263 kg/m^3) and a fully crystalline PEEK (1400 kg/m^3), respectively [26]. After that, the rule of phases was applied to calculate the theoretical densities of the composites with carbon fiber density as 1750 kg/m^3.

2.3. Differential Scanning Calorimetry (DSC)

Thermal transitions of 3D printed parts were obtained using differential scanning calorimetry (DSC3 +, Metler Toledo). Approximately 10 mg of specimens were heated from 25 to 450 °C and cooled down to 25 °C in a nitrogen atmosphere with heating and cooling rates of 10 °C/min. The glass transition temperature (T_g), melting temperature (T_m), and degree of crystallinity (X_c) were recorded. X_c was calculated from the heating scan obtained from DSC curves using Eq. (3) [27],

$$X_c = \frac{\Delta H_m}{(1-w)\ \Delta H_m^0} * 100\% \tag{3}$$

where, ΔH_m is the measured melting enthalpy, w is the weight fraction of carbon fiber, and ΔH_m^0 is the theoretical melting enthalpy corresponding to a 100% crystalline PEEK (taken as 130 J/g [26]). All reported values are the average of three measurements.

2.4. Tensile properties

Tensile properties of 3D printed specimens were determined using an Electroplus Universal Testing Machine (Instron 3366, USA) with a 10 kN load cell, crosshead velocity of 5 mm/min, and an axial extensometer of 50 mm gage length according to ASTM D638 [28]. The average of five

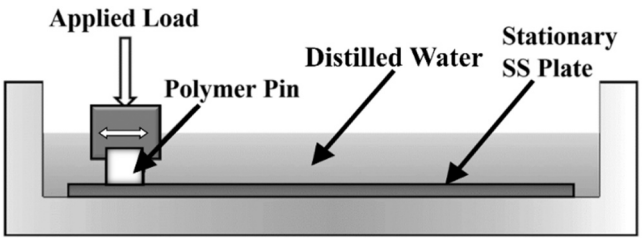

Fig. 2. Illustration of flat-on-flat tribological testing configuration.

Table 2
– Experimental conditions for tribological tests.

Testing condition	Value
Applied normal load [F_N]	80 N
Apparent contact pressure	5 MPa
Lubrication	Dry, Distilled Water
Frequency	2 Hz
Sliding speed	0.02 m/s
Stroke length	5 mm
Test duration	24 h
Total sliding distance [S_d]	1728 m
Temperature	RT (23-25 °C)
Relative humidity	~ 37%
SS plate, grade 316 L	S_a 0.25 ± 0.03 μm

Table 3 –
Characteristics of 3D printed PEEK/CF-PEEK.

Designation	Neat PEEK	PEEK10CF	PEEK20CF
Composition	Unfilled PEEK	PEEK+ 10 wt% CF	PEEK+ 20 wt% CF
Calculated theoretical density [kg/m^3]	1312	1345	1374
Measured apparent density [kg/m^3]	1291 ± 1.9	1123 ± 3.1	1127 ± 10.6
Porosity [%]	1.6	16.5	17.9
Degree of crystallinity, X_c [%]	36 ± 0.8	35 ± 0.6	30 ± 0.8
Glass transition temperature, T_g [°C]	153 ± 0.3	152 ± 0.4	152 ± 0.3
Melting temperature, T_m [°C]	339 ± 0.2	337 ± 0.5	336 ± 0.4
Ultimate tensile strength [MPa]	87 ± 1.8	94 ± 3.3	108 ± 1.1
Young's modulus [GPa]	3.4 ± 0.11	6.2 ± 0.16	8.8 ± 0.7
Elongation at break [%]	24.1 ± 1.5	5.5 ± 0.1	5.4 ± 0.05
Water absorption, 24 h@ 23 °C [%][a]	0.78	0.51	0.35

[a] Measured according to ASTM D570 [31]

repeated tests was reported for reliable and repeatable data. The tensile fractured surfaces were used to investigate the microstructure of 3D printed samples.

2.5. Tribological test setup

Cameron Plint TE77 High-Frequency Reciprocating Tribometer (Plint & Partners, Berkshire, England) with a flat-on-flat configuration was used to perform the tribological tests. A polymer pin was the moving upper specimen and a 316 L SS plate was used as a stationary counter-surface. As-printed top surfaces were used as the polymer contact face against SS without any post-processing. Testing specimens were cleaned thoroughly with ethanol and air-dried before testing. Fig. 2 illustrates the testing setup. The initial apparent contact pressure of 5 MPa was generated with an applied normal load of 80 N. Each test was conducted for 24 h with an average sliding speed of 0.02 m/s, constant throughout the test duration. The selection of contact pressure and sliding speed imitates the typical operating conditions of hydropower-bearing applications [29,30]. Table 2 lists the detailed testing conditions used. Three repeated tests were conducted to characterize the friction and wear performance with increased reliability.

2.6. Friction and wear analysis

A piezo-electric force transducer equipped with the tribometer continuously measured the friction force, whilst data-acquiring software was used to record the friction coefficients directly. A linear variable differential transformer (LVDT) sensor attached to the tribometer continuously recorded the vertical displacement of the sliding pin over the test duration. The total volume loss (ΔV) of the polymer pin was calculated using the linear wear from LVDT and the sliding surface area. The specific wear rates or wear coefficients (S_W) were determined based on Eq. (4).

$$S_W = \frac{Total\ volume\ loss\ (\Delta V)}{Applied\ normal\ load\ (F_N)\ x\ Total\ sliding\ distance\ (S_d)}\ \frac{(mm^3)}{(N.m)} \quad (4)$$

2.7. Surface characterization

A JSM-IT300 (JEOL, Peabody, USA) environmental scanning electron microscope (SEM) was utilized to investigate the worn, unworn, and fractured polymer surfaces and stainless-steel plates. Wear tracks and sliding surfaces were analyzed to study the wear mechanisms involved. Energy dispersive X-ray spectroscopy (EDS) was used to gather evidence for the possible formation of transfer layers. Polymer specimens were sputter coated with a 15 nm platinum layer before SEM analysis to prevent the charging effect.

Surface topography of the polymer pins pre- and post-tribological tests was analyzed with a scanning white-light interferometer (WLI), Zygo NewView 7300 (Connecticut, USA). A 2.5X magnification, 1X field of view, and 3.15×3.15 mm^2 scan area were used to investigate the variation of pin surface topography. 2D and 3D analysis of the surface profiles was performed with MountainsMap Premium 9 analysis software (Digital Surf, France).

2.8. FTIR

Fourier transform infrared spectroscopy (FTIR) was performed on the feedstock filaments as well as on the printed polymer surfaces before and after tribological testing using a Nicolet 380 FTIR spectrometer (Thermo Electron, Sweden). Any molecular structural changes likely to occur due to the processing and different sliding conditions were inspected. FTIR spectra were obtained as an average of 12 readings in an attenuated total reflection (ATR) mode with a wavelength range of 400–4000 cm^{-1}, 4 cm^{-1} resolution, and 128 scans. For a comparative analysis, the observed spectra were baseline-corrected and normalized to one distinct peak (1647 cm^{-1}) of the skeletal ring vibration bands.

2.9. Statistical analysis

Statistical analysis of variance (one-way and two-way ANOVA) was performed with a significance level (alpha value) of 0.05 to determine the significance of differences between the tribological results in OriginPro 2022b (origin Lab, USA).

3. Results and Discussion

3.1. Density and porosity

The measured apparent density and volumetric porosity (void content) of 3D printed specimens are presented in Table 3. The processing of neat PEEK filaments produced parts with a measured density closer to the theoretical density, contributing to the minimal void content (1.6%).

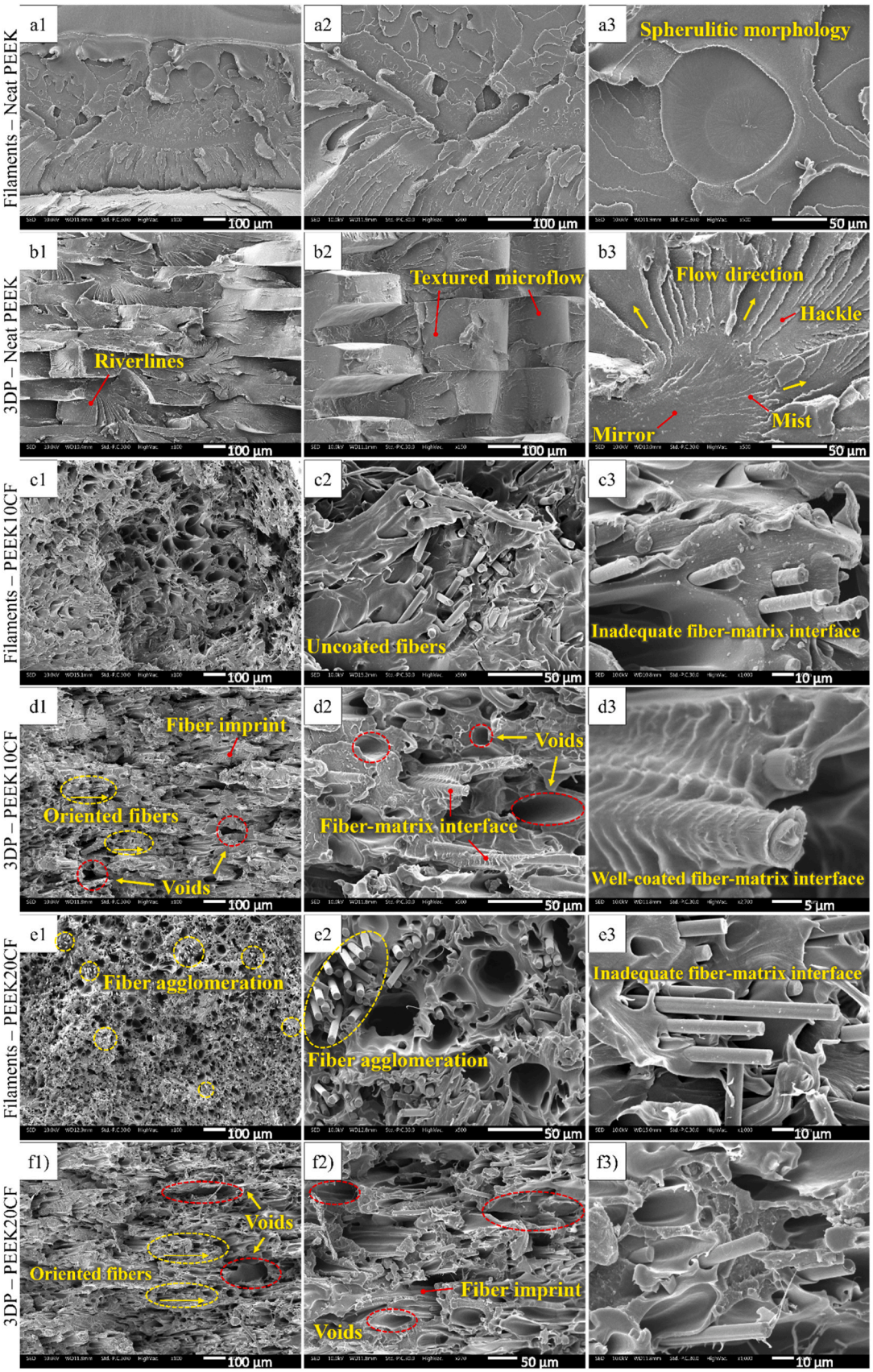

Fig. 3. Fractured surfaces: (a1, a2, a3) Neat PEEK filaments; (b1, b2, b3) 3D printed Neat PEEK; (c1, c2, c3) PEEK10CF filaments; (d1, d2, d3) 3D printed PEEK10CF; (e1, e2, e3) PEEK20CF filaments; and (f1, f2, f3) 3D printed PEEK20CF.

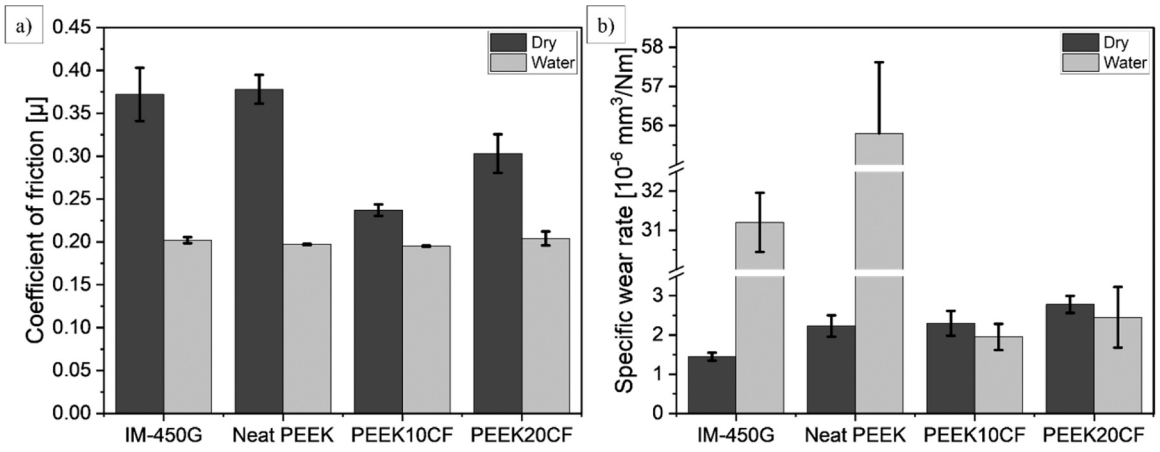

Fig. 4. Tribological results obtained under dry sliding and water-lubricated tests: (a) Average steady-state COF and (b) Specific wear rates.

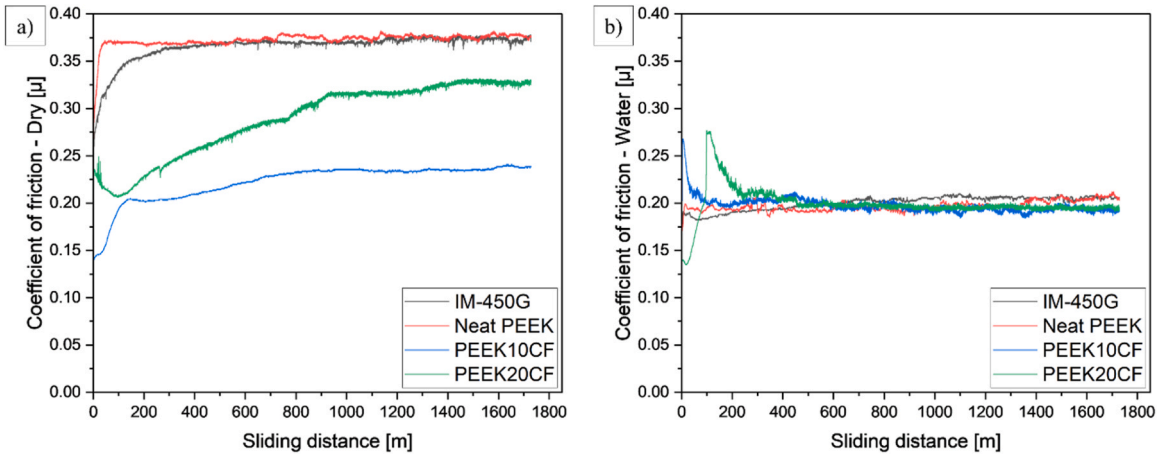

Fig. 5. Representative friction curves showing the evolution of COF with sliding distance under (a) Dry sliding and (b) Water lubrication.

The calculated theoretical densities of the printed composites increased due to the density effect of carbon fibers. However, composites exhibited reduced measured density with increasing porosity. This indicates that the experimental apparent density is dominated by the porosity. The localized fiber aggregation at higher CF contents during the filament extrusion process often results in printed parts with increased internal defects.

3.2. Differential Scanning Calorimetry (DSC)

The glass transition temperature (T_g), peak melting temperature (T_m), and degree of crystallinity (X_c) of the 3D printed specimens obtained from the first heating scan are presented in Table 3. In addition, T_g, T_m, and X_c values for the reference IM-450 neat PEEK were measured as 151 °C, 342 °C, and 34.2%, respectively. No significant differences were detected between the injection molded and 3D printed parts. This confirmed that the thermal transition parameters of neat PEEK were independent of the manufacturing methods in this study. Furthermore, the presence of CF in the PEEK matrix exhibited insignificant changes to the T_g, while T_m slightly shifted to the lower temperatures, however, the difference is not relevant compared to neat PEEK. Interestingly, it can be observed that the degree of crystallinity drops with increasing CF content, which correlates to the higher porosity observed for composites. The presence of internal irregularities in the form of voids hinders the ordered packing of molecular chains during crystallization and thus reduces the degree of crystallinity. The presence of CF in PEEK composites usually increases the degree of crystallinity due to the nucleation effect of fibers [5]. Nevertheless, CF at higher contents predominantly hinders crystal formation and lowers the crystallinity. This finding is in accordance with the literature where increasing contents of CF were reported to reduce the melting temperature and degree of crystallinity [9].

3.3. Tensile properties

The tensile properties of 3D printed specimens are listed in Table 3. It should be noted that the tensile strength of 3D printed neat PEEK in this study is lower than the reference IM neat PEEK, 87 MPa against 98 MPa (according to the supplier technical datasheet [32]). 3D printed composites exhibited improved tensile strength and modulus compared to neat PEEK, as expected. Notably, considering the FFF 3D printing, tensile properties observed in this study are satisfactory and superior to research results reported earlier [1,23,33]. It is well established that the mechanical properties of PEEK improve with the increasing degree of crystallinity [1,5]. In this study, however, printed composites with a lower degree of crystallinity showed improved tensile strength and modulus compared to neat PEEK. This is likely due to the high strength and stiffness of carbon fibers enhancing the tensile properties of neat PEEK. On the other hand, the addition of carbon fibers showed a substantial reduction in the elongation at break due to the increased brittleness of composites. This can also be associated with the fiber-matrix interfacial gaps which promote the crack initiation and propagation during tensile loading, subsequently leading to fracture without significant deformation.

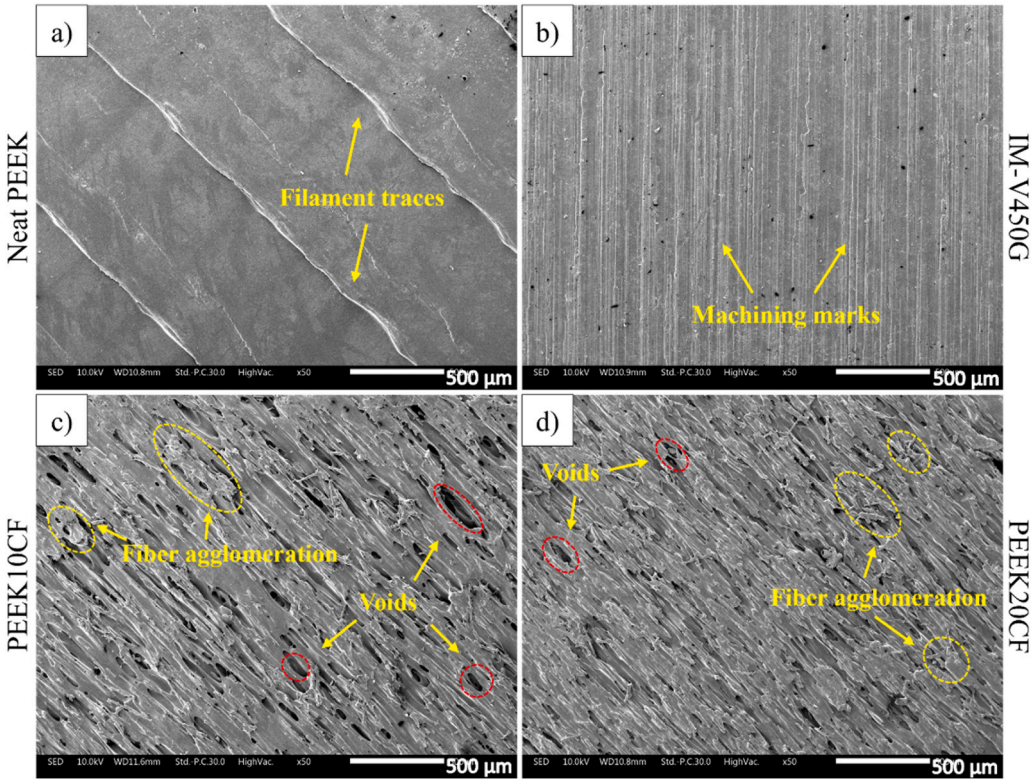

Fig. 6. SEM micrographs of unworn polymer surface: (a) 3D printed neat PEEK, (b) Injection molded neat PEEK, (c) 3D printed PEEK10CF, (d) 3D printed PEEK20CF.

3.4. Microstructure

The fractured surfaces of starting filaments and 3D printed parts were investigated using SEM. The fracture surfaces were created through tensile testing on unnotched samples, and on notched samples in the case of neat PEEK filament, due to its ductile nature. The microstructure morphology of feedstock filaments and printed parts for neat PEEK, PEEK10CF, and PEEK20CF are presented in Fig. 3. Fractured surfaces of 3D printed samples showed cleavage and rupture of layers with distinctive abrupt steps indicating brittle fracture as the primary mode of failure. Neat PEEK exhibited distinctive spherulitic morphology of crystallized PEEK, as seen in Fig. 3(a3). Regions with mirror, mist, and hackle morphology, associated with the development of riverlines from textured microflow [34], are visible in the printed neat PEEK, as seen in Fig. 3(b1-b3). 3D printed neat PEEK consisted of feather-like flowery structures with riverlines occurring from the crack propagation stretched along the fracture flow direction, Fig. 3(b3). On the other hand, composites exhibited clean matrix fracture with the presence of pulled-out fiber imprints, as illustrated in Fig. 3(d2) and Fig. 3(f2). The interface gaps between the layers due to a lack of fusion indicate insufficient consolidation during printing. The inadequate wetting and bonding of fibers with the PEEK matrix introduces gaps around the adhesion points, observed as void pockets. Composites experienced a combination of fiber-matrix debonding, matrix deformation, and crack propagation, leading to the failure of printed parts.

Internal voids and carbon fibers in the filaments are predominantly aligned parallel to the direction of extrusion, while it was parallel to the material deposition path in 3D printed parts. Voids in printed parts are formed in between the layer boundaries parallel to the build plane. As a result, layered and interconnected void networks at the interface of deposited layers are distributed from bottom to top. A detailed analysis using fractography and X-ray micro-computed tomography on the formation and distribution of internal voids in printed parts is presented in Ref. [35]. The deposition path-dependent orientation and distribution of voids and fillers often produce parts with anisotropic properties along the X, Y, and Z directions. In this regard, such internal irregularities usually initiate the localized failure of parts under stress. Stepashkin *et al.* [36] observed coarse and wide cracks after fracture with a similar pore system due to inadequate interfacial bonding of deposited layers in 3D printed CF-filled PEEK composites.

Porosity induced at the fiber-matrix interfaces due to the lack of fusion is visible in the fractured surfaces of composite filaments and printed parts. The additional porosity in the composite filaments influenced the consolidation of parts increasing the internal porosity. The dispersibility of fiber with polymer matrix determines the processing quality of filaments and consolidated composites. As carbon fibers are randomly oriented along the deposition direction during printing, such voids tend to distribute heterogeneously. The printing process improved the coating of fibers with polymer matrix enhancing the fiber-matrix bonding and interfacial adhesion. PEEK10CF feedstock filaments with closely packed morphology resulted in satisfactory wetting of fibers with polymer matrix compared to PEEK20CF. The higher content of CF in PEEK20CF filaments led to insufficient dispersion of fibers during printing, consequently resulting in an improper blending of fibers with the polymer matrix. This is reflected from the exposed fibers with large interfacial gaps in PEEK20F compared to PEEK10CF, see Fig. 3(c3, d3 versus e3, f3).

3.5. Tribological characterization

Tribological results obtained for neat PEEK and PEEK composites under dry sliding and water-lubricated conditions are presented in Fig. 4. Injection molded neat PEEK (IM-450 G) was taken as a reference to compare the tribological performance of 3D printed PEEK. Neat PEEK, irrespective of the fabrication technique, showed higher steady-state coefficients of friction reaching up to 0.40 under dry sliding against SS plates, as demonstrated in Fig. 4(a). The average 'steady-state' coefficients of friction are calculated from the last 10 h of the test duration corresponding to the 720 m sliding distance towards the end of each test. Interestingly, 3D printed neat PEEK exhibited comparable friction

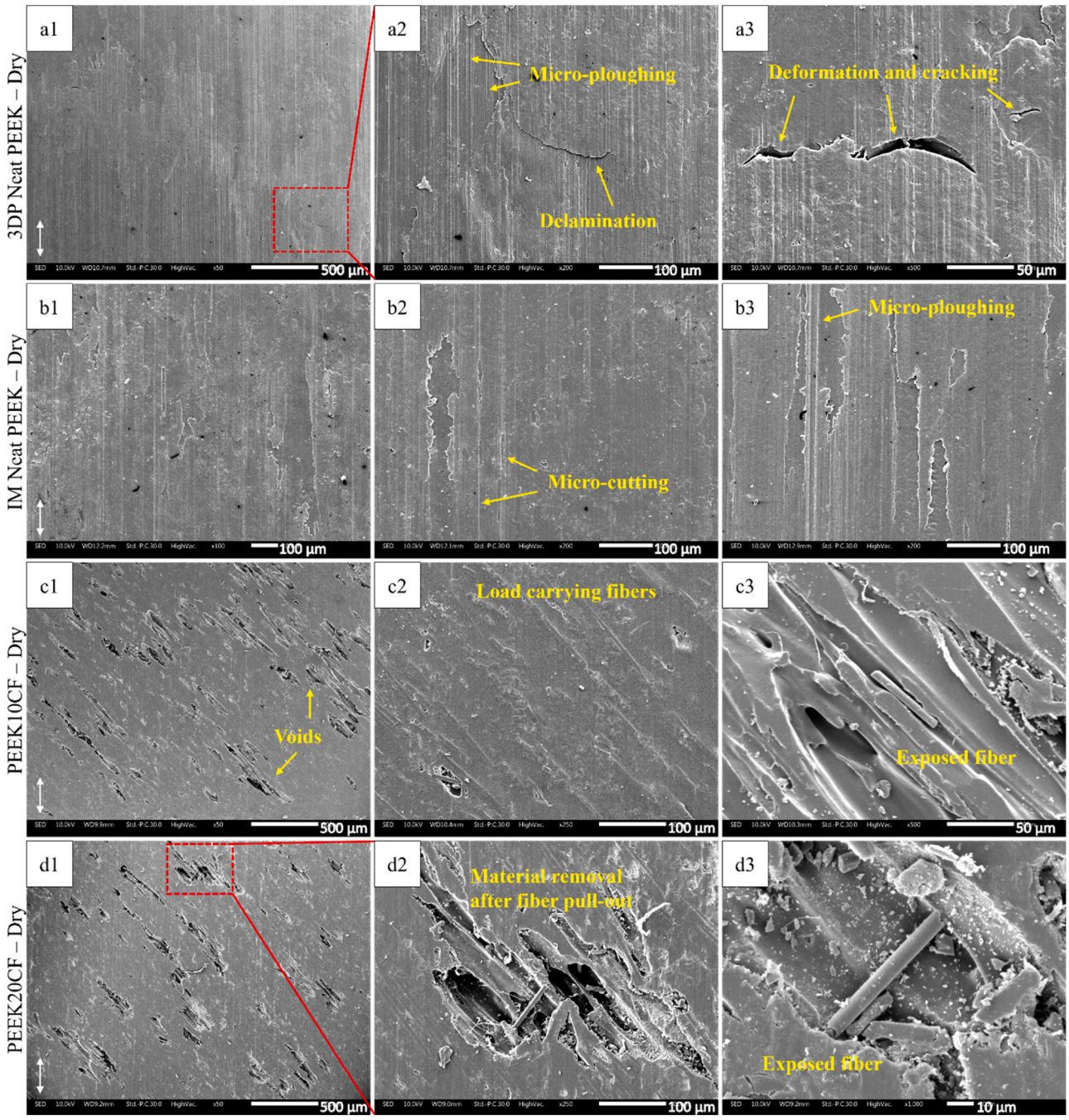

Fig. 7. SEM micrographs of worn polymer surfaces under dry sliding: (a1, a2, a3) 3D printed neat PEEK; (b1, b2, b3) Injection molded neat PEEK; (c1, c2, c3) 3D printed PEEK10CF and (d1, d2, d3) 3D printed PEEK20CF. (Double arrow indicates the sliding direction).

behavior to injection-molded neat PEEK (confirmed by one-way ANOVA with statistically insignificant differences, $p = 0.78 > 0.05$). This indicates that 3D printing can be explored as an alternative technique for the processing of high-performance thermoplastics.

The inclusion of carbon fibers with the PEEK matrix significantly improved the friction behavior under dry sliding. 3D printed composites yielded lower friction coefficients with a maximum reduction of 37% for PEEK10CF. Carbon fibers are well-known reinforcements to reduce the friction coefficients of polymer composites [8,9,37]. The inclusion of 10 wt% CF with the PEEK matrix significantly reduced the COF, while 20 wt% CF showed an increase in COF up to 0.30. The increased friction coefficients for PEEK20CF can be attributed to their higher mechanical stiffness compared to PEEK10CF, as observed earlier. Furthermore, a higher content of CF could lead to an inhomogeneous dispersion of fibers with the polymer matrix, followed by fiber agglomeration. The agglomerated contact spots act as adhesion junctions increasing the resistance to relative motion between the polymer-steel tribo pair. During dry sliding, higher energy is dissipated from the deformation of agglomerated fiber junctions overcoming the localized resistance, and resulting in increased friction coefficients [38]. The average steady-state friction for neat/composite PEEK reduced for water-lubricated conditions, exhibiting COF in the range of 0.19 – 0.21 for all tested materials. The maximum reduction of COF up to 48% was achieved for neat PEEK under water lubrication. Earlier, Unal and Mimaroglu [37] found similar friction behavior of PEEK-steel contact pairs with water lubrication compared to dry sliding. In general, polymer friction coefficients tend to

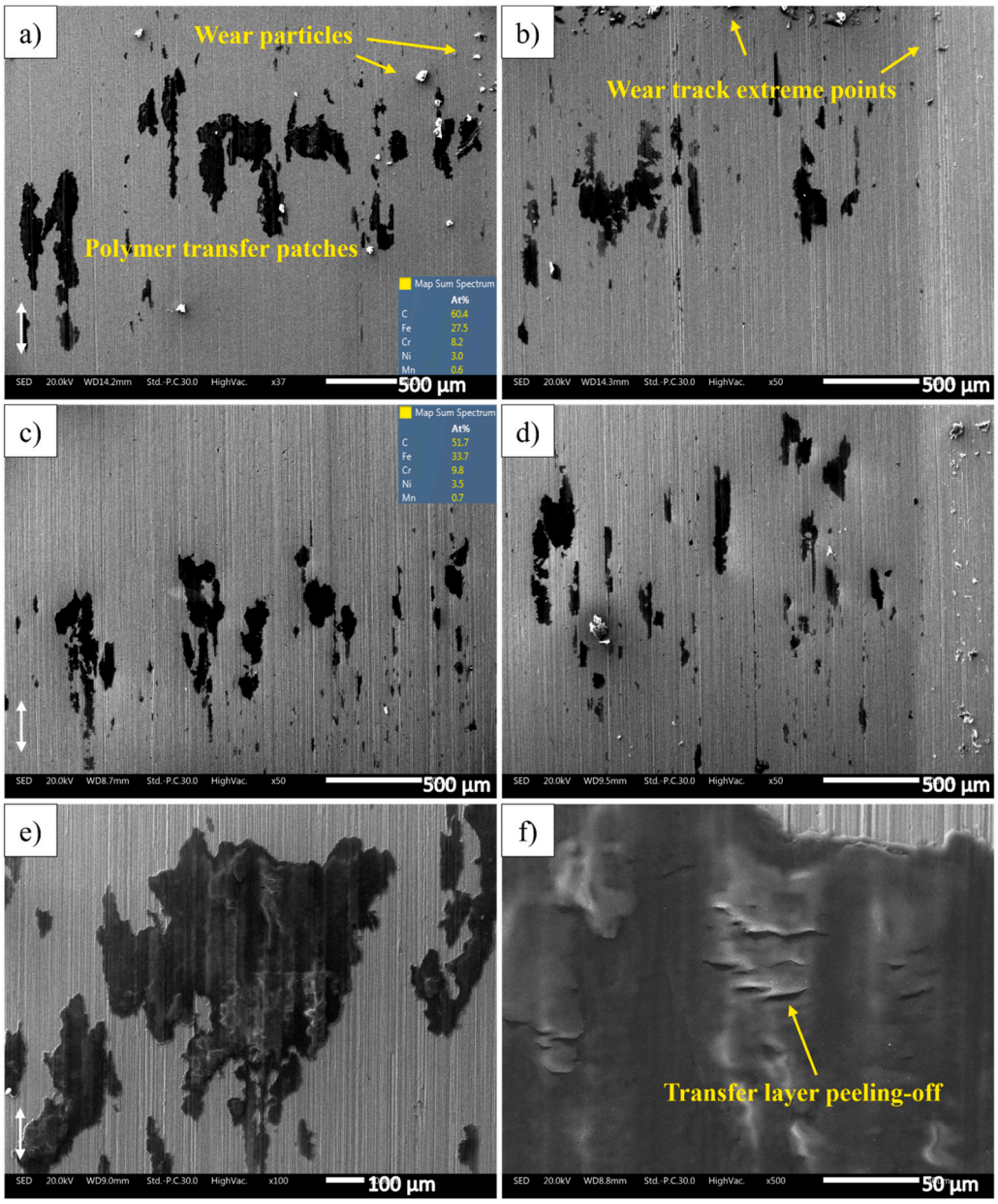

Fig. 8. Wear tracks on the countersurfaces under dry sliding: (a, b) 3D printed neat PEEK against SS and (c, d) Injection molded neat PEEK against SS; (e) Accumulation of polymer transferred to the SS under dry sliding of 3D printed neat PEEK and (f) Deterioration and cracking of transfer layers.

increase with an increase in contact temperatures due to the frictional heat induced at the interface [38,39].

The specific wear rates of neat PEEK and PEEK composites are presented in Fig. 4(b). Under dry sliding, IM neat PEEK, 3D printed neat PEEK, and PEEK composites showed specific wear rates in the order of 10^{-6} mm^3/Nm. IM neat PEEK showed better wear resistance than 3D printed neat PEEK (statistically significant differences, $p = 0.009 < 0.05$). Specific wear rates of neat PEEK in water lubrication drastically increased to the order of 10^{-5} mm^3/Nm, independent of manufacturing processes. This is likely due to the softening of unfilled PEEK induced by water up-take over the test duration. Conventional unfilled PEEK was reported to exhibit a similar reduction of wear resistance in water-lubricated sliding contacts [40]. The water absorption value for 3D printed neat PEEK (0.78%) further revealed that probable water penetration during sliding into printed neat PEEK is higher than IM neat PEEK (0.3% water absorption value was measured for reference IM-450 G). This correlates with the higher specific wear rates of printed neat PEEK compared to IM neat PEEK under water lubrication.

On the contrary, 3D printed PEEK composites showed comparable specific wear rates under both dry sliding and water lubrication (statistically insignificant differences, $p = 0.09 > 0.05$ for dry sliding and $p = 0.35 > 0.05$ for water lubrication). It can be attributed to the carbon fibers increasing the resistance to deformation of the PEEK matrix. The presence of carbon fibers on the sliding surfaces acts as the major load-bearing component and protects the polymer matrix from direct exposure and severe wear. In addition, despite the higher porosity observed for composites, relatively lower values of water absorption were observed for PEEK10CF and PEEK20CF, Table 3. This suggests that internal defects formed during printing were mainly closed system pores and are believed to have prevented easier access to water penetration from the composite surfaces. Besides, carbon fibers are inherently hydrophobic due to their low surface energy and non-polar nature, which improve the water repellent behavior of composites. It agrees with the comparable specific wear rates of printed composites under both sliding

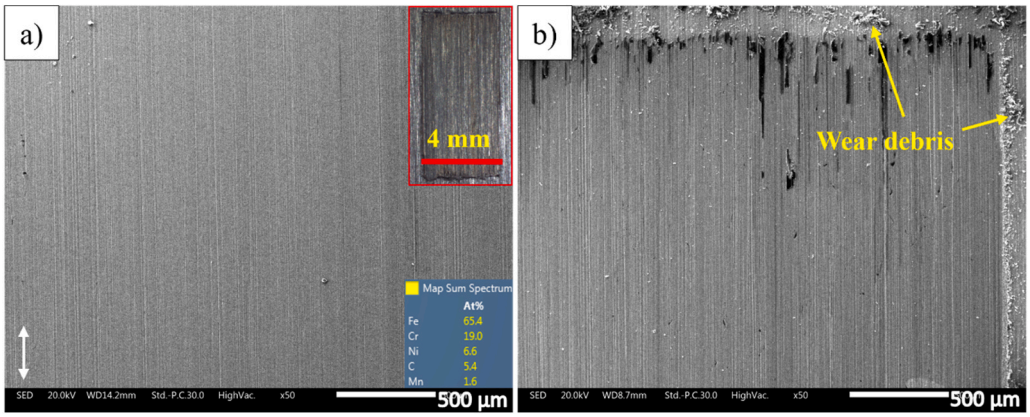

Fig. 9. Representative wear tracks formed by 3D printed PEEK composites on the countersurfaces under dry sliding: (a) SEM micrograph on the central region of wear track (Inset shows an optical micrograph of complete wear track) and (b) Trailing edges in X-Y direction of the wear track.

conditions. Moreover, it is worth mentioning that the tribological results obtained in this study did not exhibit a clear correlation with the crystallinity of tested materials. Friction characteristics, wear mechanisms, and surface topography variations of the tested materials are discussed separately for dry sliding and water-lubricated conditions hereinafter.

3.5.1. *Friction characteristics*

The representative curves showing the evolution of friction with sliding distance under dry sliding are presented in Fig. 5(a). It is clear that neat PEEK, both 3D printed and IM, showed stable coefficients of friction with a short running-in period during the test duration of 24 h. This suggests that 3D printing of neat PEEK can achieve identical friction behavior to conventional injection molding. Neat PEEK materials are capable of forming transfer layers covering the hard asperities on the steel surfaces under dry sliding [41]. This leads to a reduced resistance to motion and an early steady-state regime after achieving a balance between the formation and peeling-off of such layers. In addition, friction curves of 3D printed neat PEEK experienced minor fluctuations over the test duration. This is likely due to the multi-layer structure of the printed specimen. As material removal of the sliding layer continues, wear propagation to the subsequent layer causes variation in frictional forces, reflected as the fluctuations on friction curves. The repeated fluctuations also indicate stick-slip as well as the formation and removal of wear debris from the contact zone [42]. On the other hand, CF-filled PEEK composites showed reduced steady-state friction coefficients compared to neat PEEK. PEEK10CF yielded the lowest steady-state COF with minimal fluctuations on the friction curve. Carbon fiber reinforcement increases the strength of composites, therefore improving the resistance to ploughing and shearing of the PEEK matrix [8]. Carbon fibers further reduce the adhesion forces and stick-slip motion, consequently resulting in lower COF.

Furthermore, printed composites exhibited a longer running-in duration followed by a delayed steady-state friction regime. The friction curves stabilized after a sliding distance of around 700 and 1000 m for PEEK10CF and PEEK20CF, respectively. This can be explained by the rough contact surfaces of composites resulting in a longer duration for the deformation of rough asperities and smoothening of the sliding surfaces. Owing to the lower initial real contact area, higher pressure and shear stress are exerted on the contact points when sliding starts. As a result, higher energy is dissipated from the deformation of rough asperities to attain a smooth contact zone, consequently increasing the friction coefficients for PEEK20CF. The abrasive nature of protruding carbon fibers on the sliding surface accelerates the peeling-off of transferred polymer debris and hinders the formation of the transfer layer during dry sliding.

The evolution of coefficients of friction with sliding distance for neat PEEK and composites under distilled water lubrication is presented in Fig. 5(b). For 3D printed and IM neat PEEK, coefficients of friction start without a significant running-in period exhibiting a stable friction regime throughout the test duration. The printed composites exhibited considerable initial spikes with coefficients of friction reaching up to around 0.27, gradually reducing and stabilizing at around 0.2 after a significant running-in period. The longer running-in period for composites can be attributed to the higher surface roughness of the composites sliding against SS. The initial spikes occur due to the repeated sliding and deformation of rough asperity peaks on the composite sliding surfaces. Friction coefficients drop to a stable value with a considerable deformation of asperities and continue to be stable throughout the test. PEEK10CF attained steady-state friction after a sliding distance of around 200 m, while it was nearly 500 m in the case of PEEK20CF. In general, steady-state coefficients of friction for composites are almost identical to neat PEEK. Similar to dry sliding, friction curve fluctuations are more pronounced for neat PEEK compared to composites. The presence of carbon fibers under water lubrication did not significantly improve the friction behavior of neat PEEK in this study. However, water lubrication effectively reduced the running-in period compared to dry sliding of composites, Fig. 5. The minimized running-in period for composites under water lubrication can be attributed to the reduced frictional heating during sliding.

3.5.2. *Wear mechanisms*

Fig. 6 shows the representative micrographs of unworn polymer surfaces before tribological testing. The as-printed top surfaces of 3D printed polymers without any surface modification were used as the sliding surfaces against SS counter plates. Filament traces on the 3D printed surfaces result from the manufacturing process due to the deposition path along the $+45°/-45°$ raster angle orientation, Fig. 6 (a). Similarly, the alignment of fibers in the deposition direction is evident from the as-printed surfaces of PEEK composites, Fig. 6(c, d). In addition, voids due to the inhomogeneous dispersion of carbon fibers in the polymer matrix are visible (red dashed markings). The regions of fiber agglomeration (yellow dashed markings) are higher with PEEK20CF surfaces compared to PEEK10CF. The reference IM neat PEEK pins were machined from a rectangular injection molded block provided by Victrex. Fig. 6(b) clearly shows the machining marks on the sliding surfaces of IM neat PEEK.

SEM micrographs of worn surfaces of neat PEEK and composites under dry sliding against SS are presented in Fig. 7. It is clear that the filament traces of 3D printed neat PEEK and machining marks of IM neat PEEK were removed post-sliding. SEM micrographs of neat PEEK in Fig. 7(a1-b3) show obvious signs of abrasive and adhesive wear mechanisms under dry sliding. The presence of scratches, ploughing grooves, and cutting marks on the worn surfaces indicate abrasive wear. Polymer surfaces sliding against SS hard asperities cause micro-cutting and

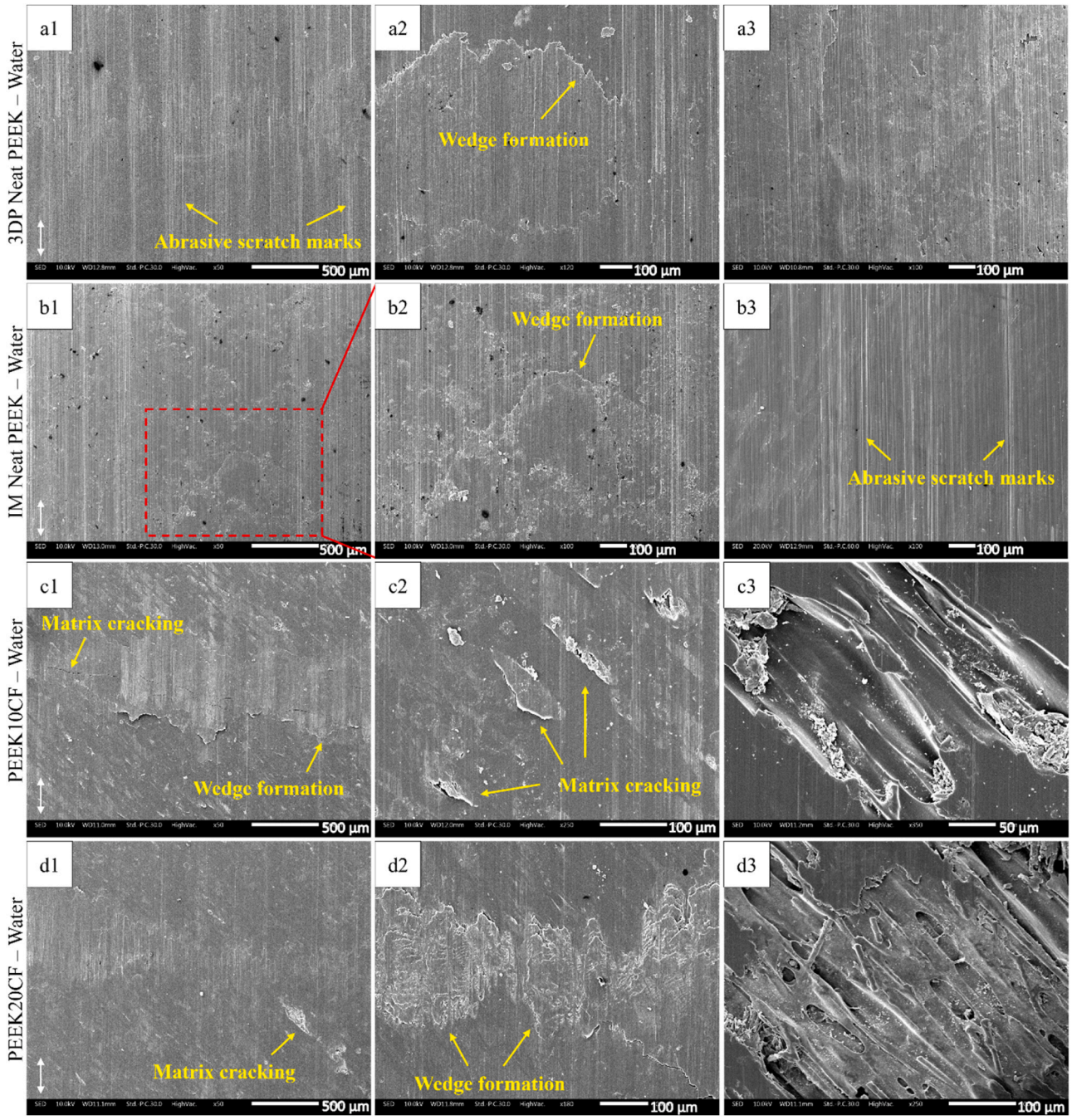

Fig. 10. SEM micrographs of worn polymer surfaces under water lubrication: (a1, a2, a3) 3D printed neat PEEK; (b1, b2, b3) Injection molded neat PEEK; (c1, c2, c3) 3D printed PEEK10CF and (d1, d2, d3) 3D printed PEEK20CF.

material removal in the form of chips or flakes. The continuous detachment of flakes from the cracked surface leads to severe damage due to delamination, Fig. 7(a2, a3), which was observed by Laux *et al.* [43] as well. Similarly, Schroeder *et al.* [44] also suggested that unfilled PEEK under reciprocating sliding exhibits a very low wear resistance and fails primarily due to the abrasion mechanism. Furthermore, 3D printed neat PEEK exhibited regions of deformation and cracking on the sliding surfaces, Fig. 7(a3). This could be the consequence of layered structure and internal micropores originating from the 3D printing process, acting as stress concentrators under repeated sliding. These cracks could lead to a higher level of thermally induced deformation and further deteriorate the interlayer bonding of the printed PEEK. In addition, the central region of printed neat PEEK surfaces experienced wedge formation resulting from the adhesion of wear debris transferred back to the polymer surfaces. The flaky debris trapped in the tribo contact in those regions tends to get reattached due to the alternating deformation during the reciprocating motion at low sliding speeds. 3D printed and IM neat PEEK exhibited a combination of abrasive and adhesive wear mechanisms. This agrees with the wear process of conventional neat PEEK surfaces observed by Voss and Friedrich [45] with the evidence of wear furrows resulting from micro-cutting and back-transferred debris.

The worn surfaces of printed composites subjected to dry sliding consisted of pits from the revealing of internal voids formed during the printing process, Fig. 7(c1, d1). The rough surface topography of as-printed composites was smoothened during the sliding. Load-carrying carbon fibers aligned along the deposition path of $+45°/-45°$ raster angle orientations are visible in Fig. 7(c2). The worn-out and exposed carbon fibers can be observed on the sliding surfaces after material

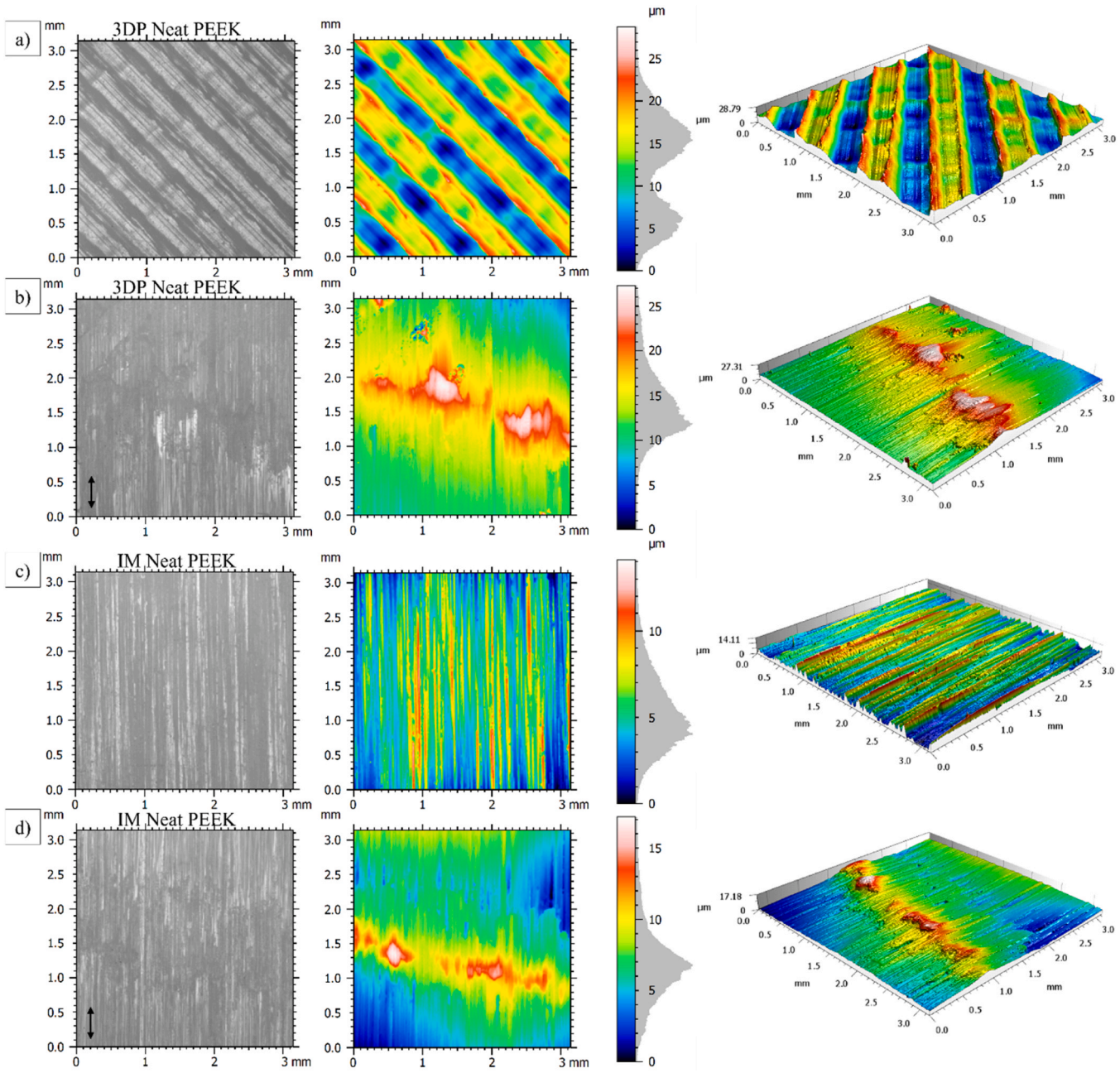

Fig. 11. Surface topography variation of neat PEEK before and after dry sliding: (a) Unworn surface of 3D printed neat PEEK; (b) Worn surface of 3D printed neat PEEK; (c) Unworn surface of IM neat PEEK and (d) Worn surface of IM neat PEEK (Double arrow indicates the sliding direction).

removal, Fig. 7(c3, d3). The exposed fibers on the surfaces indicate pull-out and fiber removal from the printed composites. The poor wetting of fibers with the polymer resin observed in Fig. 7(c3, d3) suggests an inadequate filler-matrix interface. PEEK20CF showed severely damaged regions and relatively larger pits compared to PEEK10CF after the sliding duration. The removal of large fragments of polymer flakes due to fiber pull-out is more pronounced with PEEK20CF, Fig. 7(d2, d3). Relatively higher agglomeration of carbon fibers on the PEEK20CF experiences higher shear stress in the interfacial zone and accelerates the material removal during sliding. Composite surfaces exhibited no signs of adhesive wear compared to neat PEEK under dry sliding. This can be attributed to the increased bulk thermal conductivity of composites with the presence of carbon fibers. The improved transfer of frictional heat away from the composite surfaces reduces the thermal softening and matrix deformation during dry sliding [46]. In general, surface damage phenomena for 3D printed neat/composite PEEK agree with earlier studies reported for conventional neat/composite PEEK where cracking and delamination were found as the major wear mechanisms [47,48].

Fig. 8 shows the wear tracks formed on the SS countersurface under dry sliding of 3D printed and IM neat PEEK. Wear tracks contained discontinuous and patchy layers of polymers transferred on the SS plates. The presence of high carbon content from EDS analysis confirmed that the patches were transferred from the polymer pins, Fig. 8(a, c). The transfer layers formed during dry sliding protect the bulk polymer from the abrasive action of hard steel surfaces and reduce the wear rate. The coverage of polymer transfer was mostly observed near the trailing edges of sliding pins on the wear tracks. The patches tend to distribute along the sliding direction of polymer pins. The sliding velocity of the polymer pin at the start and end of the stroke goes to almost zero allowing for the accumulation of wear particles at the

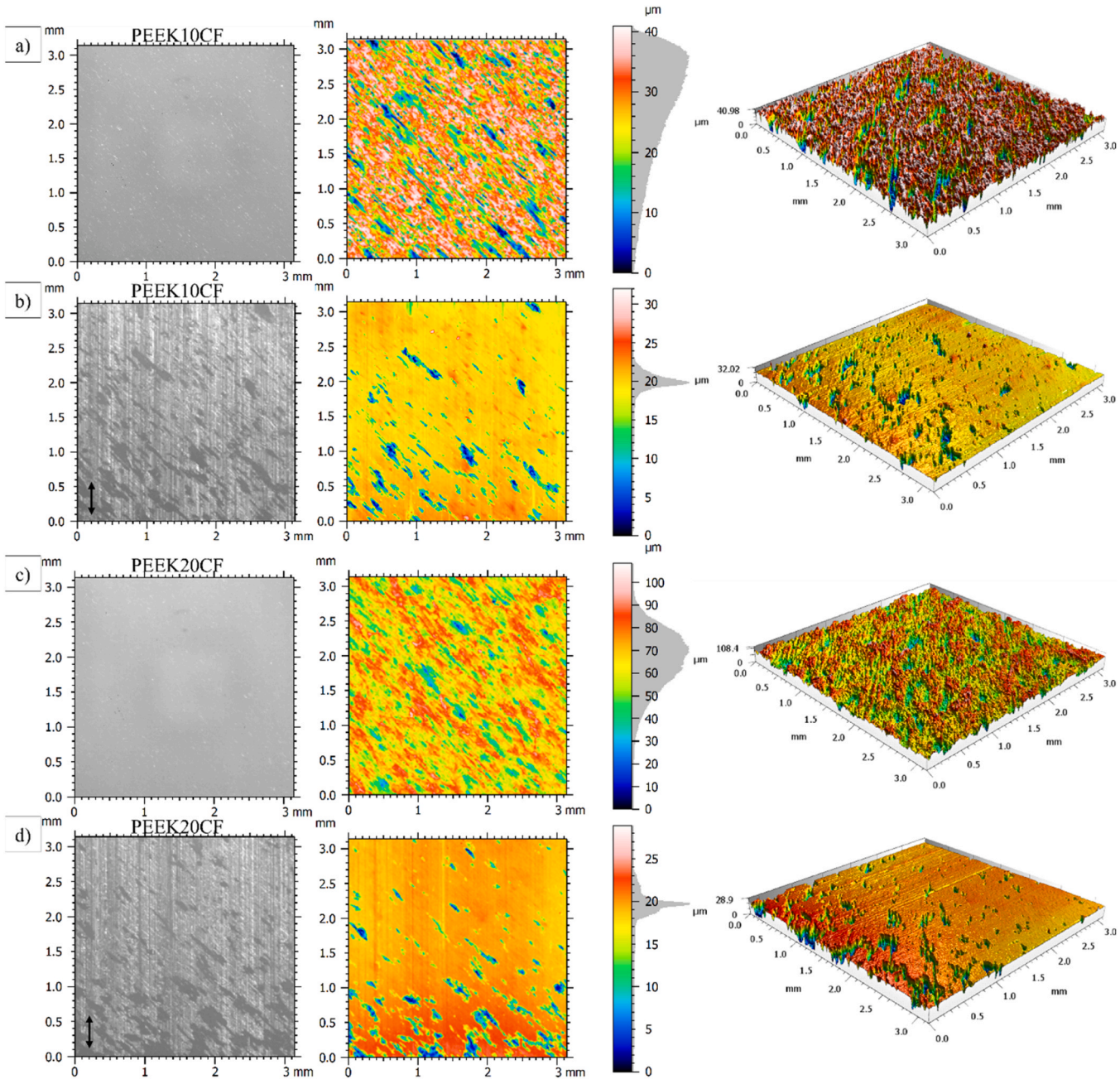

Fig. 12. Surface topography variation of composites before and after dry sliding: (a) Unworn surface of PEEK10CF; (b) Worn surface of PEEK10CF; (c) Unworn surface of PEEK20CF and (d) Worn surface of PEEK20CF.

trailing edges. The central region of the wear track lacks any pronounced patches of polymer transfer, supporting the adhesion of wear particles back to the polymer surfaces in such regions as observed earlier in Fig. 7. A closer inspection of such patches indicated a potential deterioration phenomenon of the transferred layers during the test, Fig. 8(e, f). The adhesion of worn polymer lumps detached from the pin onto the countersurface forms a transfer layer. If this layer is thin and held between the contact, steady friction and wear are attained [49]. However, under repeated reciprocating sliding, the transferred layer starts to deform, crack, and eventually peel off from the countersurface. This leads to a continuous cycle of deposition and removal of polymer patches on the countersurface which prevents the formation of stable and durable transfer layers. Laux *et al.* [43] suggested that non-uniform patches of wear debris on the counter surface could cause the fluctuations of COF with PEEK-steel contacts.

Fig. 9 shows the representative wear tracks formed by 3D printed composites sliding against SS under dry sliding. Wear tracks formed by both PEEK10CF and PEEK20CF lacked substantial formation of transfer layers, except for minor deposits near the trailing edges. This could be either due to the composites being incapable of forming a transfer layer or the rapid removal of transferred material. The latter is believed to be the governing factor in this case, as the abrasive carbon fibers present at the polymer sliding surfaces speed up the peeling-off process of transferred polymers. It was earlier suggested that CF-filled PEEK is capable of forming thin and smooth transfer layers onto the countersurface, while the coverage may vary depending on the countersurface material [50].

The worn surfaces of neat PEEK and composites sliding against SS under water lubrication are presented in Fig. 10. The worn surfaces exhibited a polishing effect with visible marks of scratching and

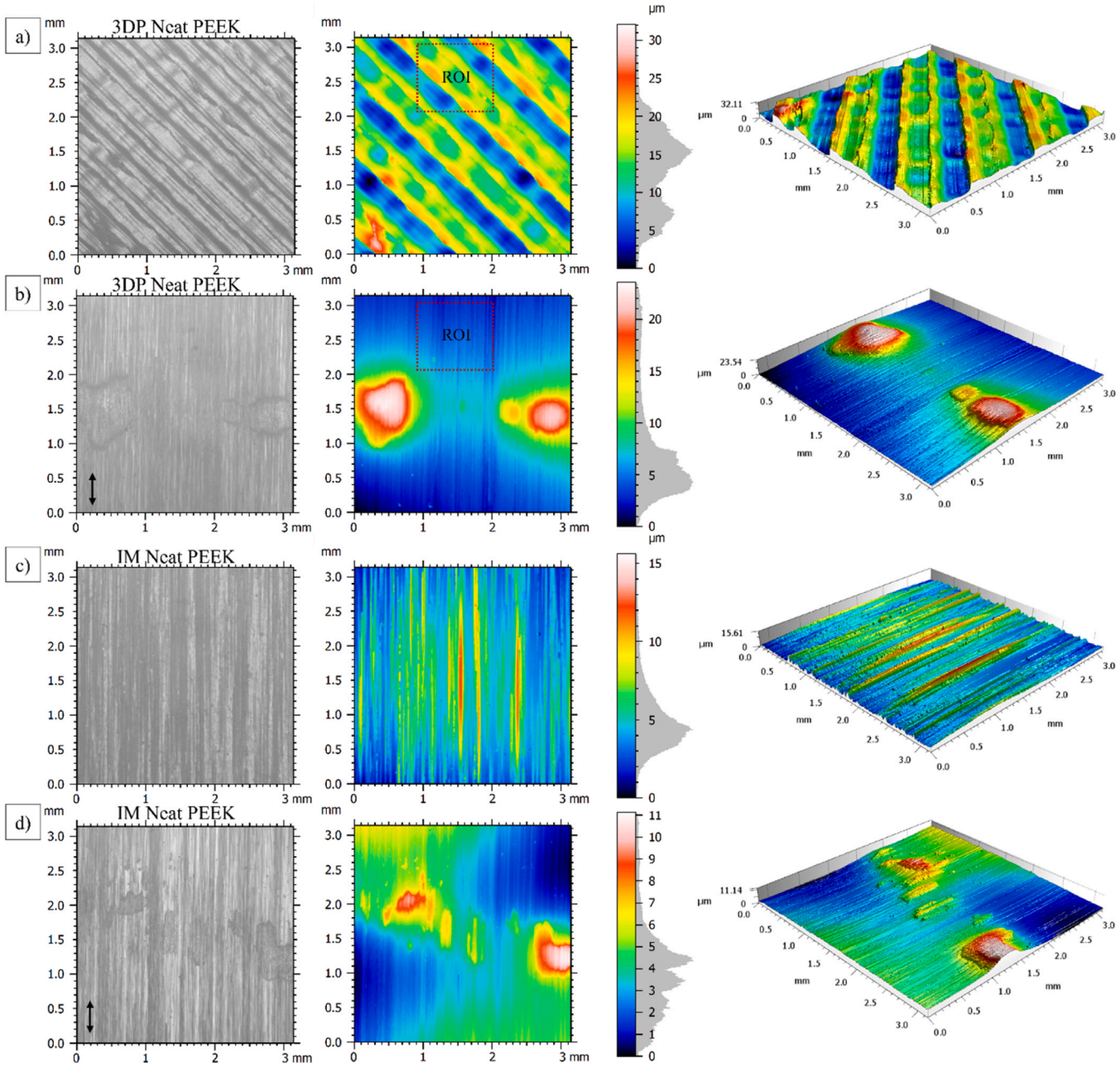

Fig. 13. Surface topography variation of neat PEEK before and after water-lubricated tests: (a) Unworn surface of 3D printed neat PEEK; (b) Worn surface of 3D printed neat PEEK (ROI: region of interest within 1 mm x 1 mm scan area of 3D printed neat PEEK); (c) Unworn surface of IM neat PEEK and (d) Worn surface of IM neat PEEK.

ploughing during sliding. Both 3D printed and IM neat PEEK exhibited minor indications of wedge formation, Fig. 10(a1-b3), similar to dry conditions. However, the coverage is smaller as water lubrication restricts the adhesive bonding of wear debris back to the polymer surface. Golchin *et al.* [51] suggested that agglomeration of wear debris forms large and brittle particles under water lubrication further accelerating the wear process of neat PEEK polymers. The sliding surfaces in this study experienced relatively homogeneous abrasive wear under water lubrication, with adhesive wear limited to only minor contact points concentrated mostly around the central region, Fig. 10(a1, b1). Water lubrication enhances the flush out of wear debris from the contact zone and restricts the formation of protective layers, leaving the polymer surface vulnerable to direct contact against SS. This was supported by the wear tracks lacking any evidence of transfer layer formation on the countersurface under water lubrication. As a result, micro-ploughing and abrasive action of the hard asperities of steel surfaces cause scratch marks to appear on the polymer surfaces along the direction of sliding, Fig. 10(a3, b3). In addition, water absorption further softens the polymers and accelerates the wear under shear stress due to reciprocating sliding. This leads to relatively higher wear rates of unfilled polymer surfaces under water lubrication than dry sliding.

The worn surfaces of printed composites after the test duration under water lubrication are presented in Fig. 10(c1-d3). In contrast to dry sliding, the composites subjected to water lubrication indicated adhesive wear with signs of polymer back-transfer. Interestingly, the back transfer of wear debris on the composite surfaces is more prominent around the central region under water lubrication. Wedge formation and matrix cracking followed by delamination were observed as the dominant wear mechanism. The repeated formation, growth, and shearing of adhesion junctions on the sliding surfaces accelerate the wear process.

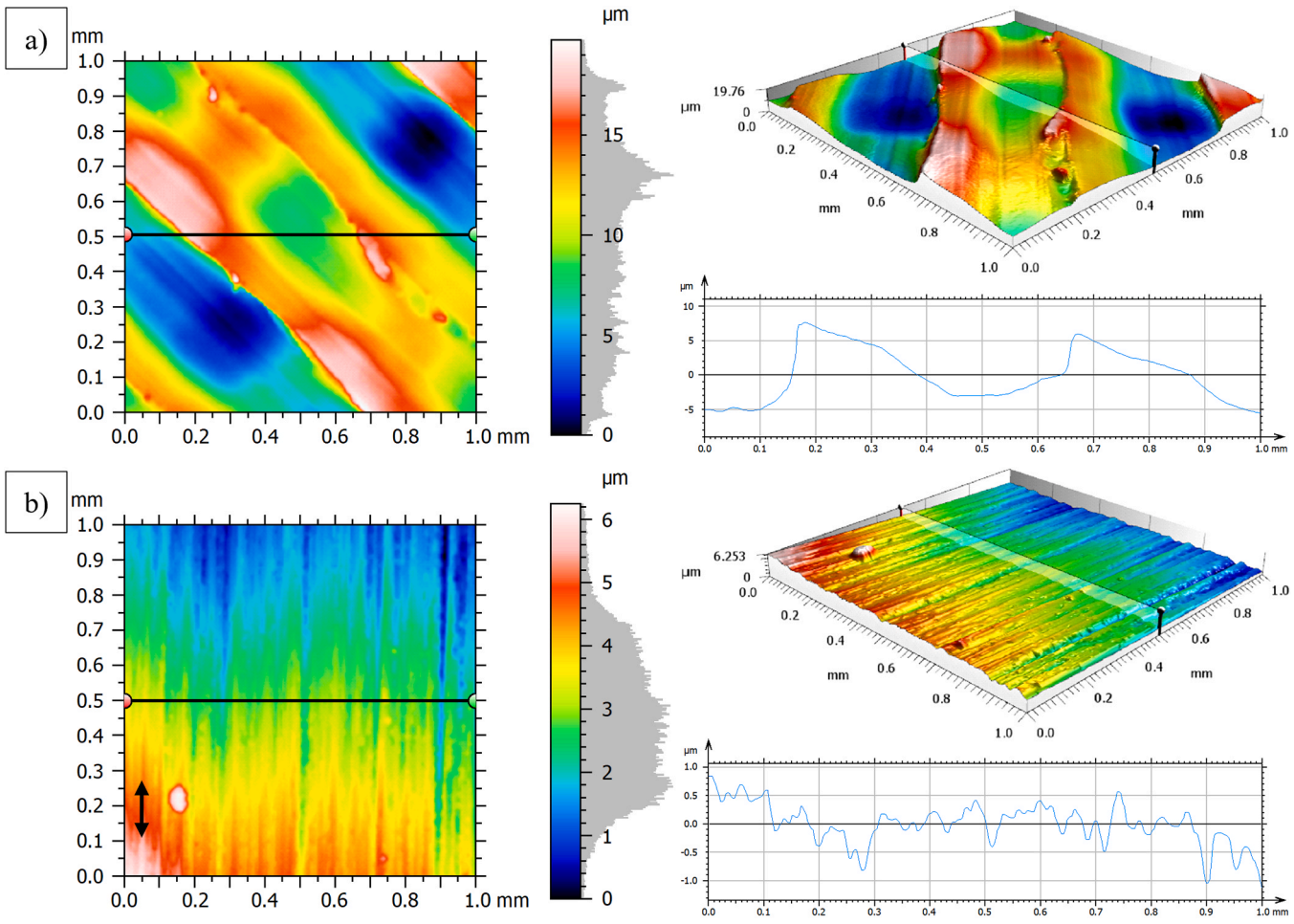

Fig. 14. ROI of 3D printed neat PEEK from Fig. 13 sliding under water lubrication showing the surface topography variation within a 1 mm x 1 mm scan area lacking back transferred material: (a) Unworn surfaces before water lubricated tests and (b) Worn surfaces after water lubricated tests.

PEEK20CF consisted of regions with severely delaminated surfaces after the test duration compared to PEEK10CF, illustrated in Fig. 10(c3, d3), reflecting the relatively higher specific wear rates of PEEK20CF. Water-lubricated composites showed surfaces with relatively lower content of exposed voids and pits after the test duration compared to dry sliding conditions, Fig. 10(c1, d1) and Fig. 7(c1, d1). This can be attributed to the reduced contact temperature of the tribo-system under water lubrication, minimizing the friction and consequently wear.

3.5.3. *Surface topography variations*

Surface topography variations of 3D printed neat PEEK and IM neat PEEK before and after the test duration are presented in Fig. 11. 2D and 3D surface analysis of the polymers before and after dry sliding strongly correlates with the observation from SEM, in Fig. 7. The presence of hills and pits occurring from the deformation and cutting is visible post-sliding, Fig. 11(b, d). 3D printed neat PEEK experienced surface roughness variation, from a S_q of 5.6 to 3.6 μm after dry sliding, while a minor change was measured for IM neat PEEK, from a S_q of 2 to 2.3 μm. The maximum profile heights (S_z) of 3D printed and IM neat PEEK changed from 28.8 to 29.2 μm and 14.1 to 17.2 μm, respectively. The increase in profile heights post-sliding indicates the adhesion of wear debris back to the polymer surfaces, mostly scattered around the central region and stretched along the sliding direction.

Surface topography variations of printed composites under dry sliding are presented in Fig. 12. The protruding fibers resulted in higher surface roughness of composites compared to that of printed neat PEEK. Composites showed spots on the pre-sliding surfaces indicating fiber agglomeration during the dispersion in the polymer matrix. PEEK20CF included a higher degree of peaks and valleys compared to PEEK10CF, Fig. 12(a) compared to Fig. 12(c). 2D and 3D analysis of surface profiles showed smoothening of composites after sliding against SS. Surface roughness (S_q) of PEEK10CF and PEEK20CF after dry sliding changed from 8.4 to 3 μm and 12.4 to 3.3 μm, respectively. Similarly, maximum profile heights (S_z) for PEEK10CF and PEEK20CF changed from 41 to 32 μm and 108.4 to 29 μm, respectively. Surface topography in some regions indicated the packing of voids with the wear debris trapped in the contact zone during dry sliding. Newer pits were revealed on the post-sliding surfaces from the existing internal voids.

Surface topography variations of 3D printed and IM neat PEEK before and after sliding under water lubrication are presented in Fig. 13. 2D and 3D analysis of neat PEEK surfaces under water lubrication indicated similar features post-sliding as observed from SEM micrographs in Fig. 10. The severity of wedge formation is more pronounced with 3D printed neat PEEK compared to IM neat PEEK under water lubrication. This could be due to the manufacturing process and the impact of a layered structure of printed polymers under sliding. Surface modification from micro-cutting and micro-ploughing marks are noticeable on both 3D printed and IM neat PEEK post-sliding. Surface roughness (S_q) for printed neat PEEK changed from 5 to 4.5 μm, while it remained unchanged for IM neat PEEK at around 1.7 μm. On the other hand, the maximum profile heights (S_z) for printed and IM neat PEEK changed from 32.1 to 23.5 μm and 15.6 to 11.1 μm, respectively. This suggests that even though almost no change was observed with the surface roughness values, characteristics of the surface profile and

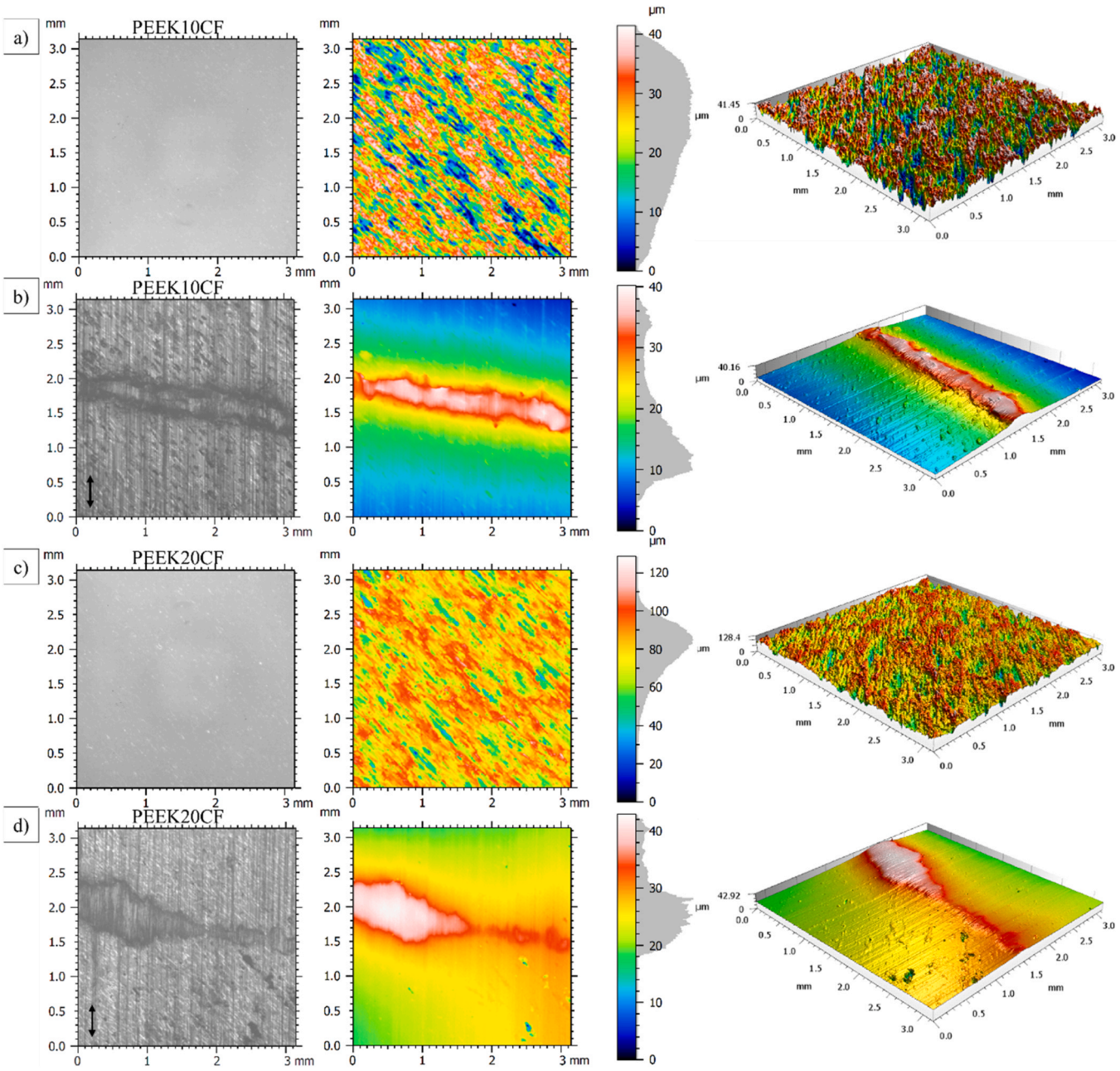

Fig. 15. Surface topography variation of composites before and after water-lubricated tests: (a) Unworn surface of PEEK10CF; (b) Worn surface of PEEK10CF; (c) Unworn surface of PEEK20CF and (d) Worn surface of PEEK20CF.

texture modified considerably post-sliding. 3D analysis exhibiting a larger variation of maximum profile heights (S_z) in Fig. 13 indicated severe wear of neat PEEK under water lubrication, in contrast to dry sliding, as observed earlier in Fig. 11. In addition, surface analysis of 3D printed neat PEEK further elucidates the relatively stronger wedge formation phenomenon under water lubrication. The back transferred polymer confined to the right and left extremes on the central region of the sliding pin is highly accentuated in Fig. 13(b) versus Fig. 11(b).

To further understand the topography variation without the wedge formation, a region of interest (ROI) for 3D printed neat PEEK from Fig. 13(a, b) lacking any significant back-transferred material was selected. Surface profile analysis of the ROI within a 1 mm x 1 mm scan area, presented in Fig. 14, showed a larger variation post-sliding. The surface roughness (S_q) reduced from 4.6 to 1 μm, while the maximum profile height (S_z) reduced from 19.8 to 6.3 μm. In addition, a slicing profile perpendicular to the sliding direction exhibited the change in peak-to-valley height (R_z) from 11.4 to 1.4 μm post sliding. The variation of peak height (R_p = 7 to 0.6 μm) and valley depth (R_v = 4.4 to 0.8 μm) showed that the polymer surface asperities were significantly smoothened within the scan area. Thereby, water lubrication resulted in notably polished surfaces of 3D printed neat PEEK after sliding against SS for 24 h.

Fig. 15 presents the surface topography variations of 3D printed composites. The scratch marks from the micro-cutting of sliding surfaces are visible for both composites. The surface roughness (S_q) for PEEK10CF changed from 9.2 to 7.8 μm post sliding, while the same for PEEK20CF was 13.4 to 5.1 μm. This suggests that the polishing action was severe for PEEK20CF. The back-transferred wear debris was mostly confined to the central region for both composites. After the test duration, such regions for PEEK10CF seemed uniformly distributed perpendicular to the sliding direction, while PEEK20CF exhibited non-uniform coverage. The presence of pits occurring due to material removal was

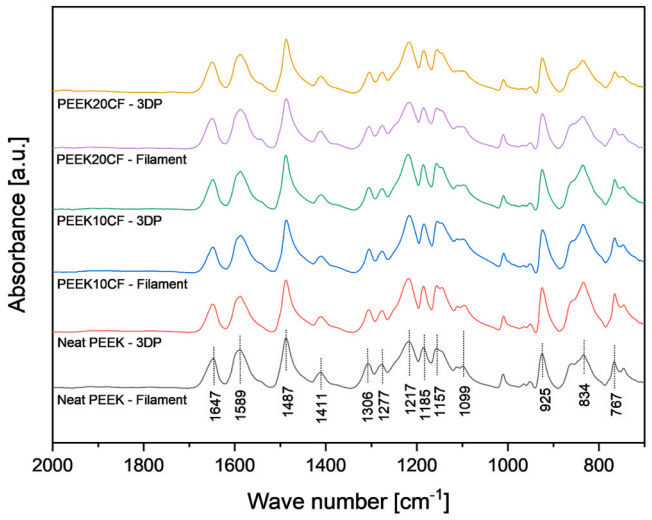

Fig. 16. FTIR spectra of starting filaments versus 3D printed PEEK-based materials.

Table 4
– FTIR peak assignment of PEEK-based materials.

Assignment	Wavenumber [cm^{-1}]
C═O carbonyl stretching in ketone	1647
phenyl ring stretching	1589, 1487, 1411
carbonyl group of ketone linkage	1306
asymmetric stretching of diphenyl ether	1277, 1217, 1185
in-plane stretching vibration of C–H	1157, 1099
diphenyl ketone band	925
out-of-plane bending vibration of C–H in benzene	834, 767

observed for PEEK20CF in Fig. 15(d), which resonates with the SEM observation in Fig. 10(d3).

3.6. FTIR

The characteristic FTIR spectra observed for starting filaments and printed parts showed no noticeable differences, Fig. 16. The assignments for corresponding peaks are provided in Table 4 [52]. FTIR spectra of printed parts showed no evidence of localized oxidation originating from the printing process, confirming that the manufacturing process had no impact on the molecular structure of deposited materials.

Furthermore, FTIR spectra of 3D printed samples before and after the tribological testing were analyzed for possible chemical changes due to the sliding against SS. From Fig. 17, no obvious changes and alterations of ketone and ether groups associated with PEEK were observed. The significant spectral features and peak positions in the spectra of neat PEEK remained unchanged for all materials after sliding against steel. Interestingly, samples after dry sliding tests showed a relatively weak band signal in the carbonyl region around 1800–1700 cm^{-1}, zone 1 in Fig. 17(a). The changes in FTIR spectra in the carbonyl region at 1800–1675 cm^{-1} for tribo-tested samples were inspected. A closer examination of the spectra revealed an appearance of a new peak with a maximum centered at 1734 cm^{-1}, Fig. 17(b), usually not associated with PEEK. Sliding could promote changes in the chemical structure of PEEK due to oxidation or crosslinking in PEEK-steel tribo contacts [39,53]. The appearance of a new absorption band around 1740–1730 cm^{-1} may suggest some degree of molecular structural change of PEEK, possibly due to oxidation at the interface zone during dry sliding.

Studies focused on the thermal aging of PEEK in air atmosphere have reported distinct signs of thermo-oxidative degradation with the appearance of new peaks associated with easter groups in the carbonyl region around 1740–1730 cm^{-1} [52,54]. Cole and Casella [52,55] identified the absorption band at 1739 cm^{-1} for PEEK films and CF-filled PEEK composites heated in air at 400 °C, associated with the formation of phenyl benzoate by the oxidation of original carbonyl groups. Courvoisier *et al.* [56] also observed a similar band with long-duration heating at 250–320 °C due to the diffusion of oxygen into PEEK. On the other hand, no signs of phenyl benzoate bands were observed at

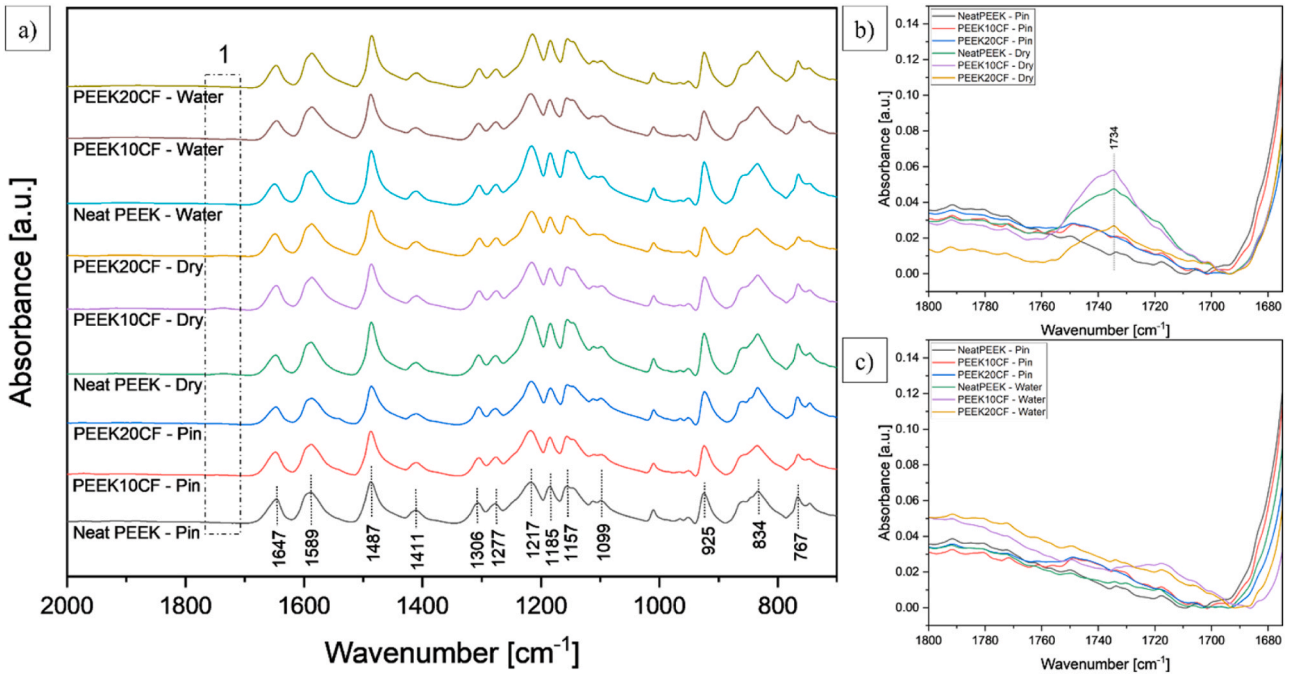

Fig. 17. FTIR spectra of 3D printed PEEK-based materials: (a) Before and after tribological testing under dry sliding and water lubrication; (b) Carbonyl region (1800–1675 cm^{-1}) in dry sliding; and (c) Water lubricated conditions.

rapid high-temperature processing of PEEK [57]. The disappearance of phenyl benzoate bands was likely due to the shorter duration available for the oxygen to diffuse into PEEK at higher temperatures above 400 °C. This also explains the lack of a 1739 cm^{-1} peak on the spectra of PEEK printed at 440 °C, as the deposited materials do not remain in a molten state for a longer duration to facilitate thermal oxidation.

However, its appearance after dry sliding tests in this study could indicate changes originating from the friction-induced diffusion of oxygen into the PEEK under repeated sliding for a duration of 24 h. Also, the growth of this peak is dependent on the differences in the energy dissipation during sliding at different conditions and temperatures. During dry sliding, higher energy is dissipated from the system due to relatively higher frictional heating compared to water lubrication, which could explain the absence of this peak on the spectra of samples tested under water-lubricated conditions, Fig. 17(c).

4. Conclusions

Neat PEEK and CF-PEEK composites were additively manufactured using the material extrusion-based FFF technique. Experimental investigations on porosity, thermal properties, tensile properties, and tribological performances were carried out. A comprehensive analysis of friction characteristics and wear mechanisms under dry sliding and water-lubricated conditions was conducted. The conclusions of this work can be highlighted as follows.

- FFF 3D printing can produce neat PEEK and CF-PEEK composites with satisfactory thermal and tensile properties. Microstructure morphology and surface topography analysis confirmed that the orientation and distribution of porosity and carbon fibers were dependent on the material deposition path during the printing process.
- 3D printing of PEEK-based components achieved similar friction and wear mechanisms to conventional injection molding of PEEK. PEEK reinforced with 10 wt% carbon fiber was optimal considering the tribological performance.
- Under dry sliding, CF-PEEK composites yielded lower COF than neat PEEK, with a maximum reduction of 37% for PEEK10CF. Water lubrication further reduced the COF compared to dry sliding, with a maximum reduction of 48% for 3D printed neat PEEK.
- 3D printed neat/composite PEEK under dry sliding showed comparable specific wear rates to IM neat PEEK in the order of 10^{-6} mm^3/Nm. Water lubrication increased the specific wear rates of neat PEEK by an order to 10^{-5} mm^3/Nm, whereas almost no change was observed for composites.
- A combination of abrasive and adhesive wear mechanisms was observed for neat PEEK, while composites revealed fiber-matrix debonding, matrix deformation, and delamination during sliding.

The main scientific contribution of this study is a better understanding of the tribological performance of FFF 3D printed PEEK-based materials. The findings indicate the potential of extrusion-based AM as an alternative processing technique for polymers in bearing applications. The impact of different types and contents of nano/micro fillers on the 3D printing of high-performance composites to achieve improved tribological performance can be explored in the future.

Statement of originality

The authors confirm that the research paper is original and has not been published previously or considered for publication elsewhere, and if accepted it will not be published elsewhere.

CRediT authorship contribution statement

Dhakal Nayan: Conceptualization, Methodology, Investigation, Data curation, Formal analysis, Validation, Visualization, Writing – original draft. **Espejo Cayetano:** Supervision, Writing – review & editing. **Morina Ardian:** Supervision. **Emami Nazanin:** Conceptualization, Project administration, Resources, Funding acquisition, Supervision, Writing – review & editing.

Declaration of Competing Interest

The authors declare that they have no known competing financial interests or personal relationships that could have appeared to influence the work reported in this paper.

Data Availability

Data will be made available on request.

Acknowledgements

The authors would like to thank the European Union's Horizon 2020 research and innovation programme for funding this research under the GreenTRIBOS, Marie Skłodowska-Curie grant agreement No. 860246. The authors are grateful to Victrex™ for providing the injection molded reference material.

References

[1] Zanjanijam AR, Major I, Lyons JG, Lafont U, Devine DM. Fused filament fabrication of PEEK: a review of process-structure-property relationships. Polymers 2020;12 (8). https://doi.org/10.3390/polym12081665.
[2] Altıparmak SC, Yardley VA, Shi Z, Lin J. Extrusion-based additive manufacturing technologies: state of the art and future perspectives. J Manuf Process 2022;83: 607–36. https://doi.org/10.1016/j.jmapro.2022.09.032.
[3] Das A, Chatham CA, Fallon JJ, Zawaski CE, Gilmer EL, Williams CB, et al. Current understanding and challenges in high temperature additive manufacturing of engineering thermoplastic polymers. Addit Manuf 2020;34. https://doi.org/10.1016/j.addma.2020.101218.
[4] Park S, Fu K. Polymer-based filament feedstock for additive manufacturing. Compos Sci Technol 2021;213. https://doi.org/10.1016/j.compscitech.2021.108876.
[5] Kurtz S.M., *PEEK Biomaterials Handbook*. 2019. DOI: ⟨https://doi.org/10.1016/C2016–0-02479–8⟩.
[6] Nunez EE, Gheisari R, Polycarpou AA. Tribology review of blended bulk polymers and their coatings for high-load bearing applications. Tribology Int 2019;129: 92–111. https://doi.org/10.1016/j.triboint.2018.08.002.
[7] Kurdi A, Chang L. Recent advances in high performance polymers—tribological aspects. Lubricants 2018;7(1). https://doi.org/10.3390/lubricants7010002.
[8] Flöck J, Friedrich K, Tuan Q. On the friction and wear behaviour of PAN- and pitch-carbon fiber reinforced PEEK composites. Wear 1999;225-229:304–11. https://doi.org/10.1007/s11249-015-0520-7.
[9] Li F, Hu Y, Hou X, Hu X, Jiang D. Thermal, mechanical, and tribological properties of short carbon fibers/PEEK composites. High Perform Polym 2017;30(6):657–66. https://doi.org/10.1177/0954008317715313.
[10] Kalin M, Zalaznik M, Novak S. Wear and friction behaviour of poly-ether-ether-ketone (PEEK) filled with graphene, WS 2 and CNT nanoparticles. Wear 2015;332-333:855–62. https://doi.org/10.1016/j.wear.2014.12.036.
[11] Puértolas JA, Castro M, Morris JA, Ríos R, Ansón-Casaos A. Tribological and mechanical properties of graphene nanoplatelet/PEEK composites. Carbon 2019; 141:107–22. https://doi.org/10.1016/j.carbon.2018.09.036.
[12] Laverne F, Marquardt R, Segonds F, Koutiri I, Perry N. Improving resources consumption of additive manufacturing use during early design stages: a case study. Int J Sustain Eng 2019;12(6):365–75. https://doi.org/10.1080/19397038.2019.1620897.
[13] Gebler M, Schoot Uiterkamp AJM, Visser C. A global sustainability perspective on 3D printing technologies. Energy Policy 2014;74:158–67. https://doi.org/10.1016/j.enpol.2014.08.033.
[14] Mani M, Lyons KW, Gupta SK. Sustainability characterization for additive manufacturing. J Res Natl Inst Stand Technol 2014;119:419–28. https://doi.org/10.6028/jres.119.016.
[15] Gao G, Xu F, Xu J, Tang G, Liu Z. A survey of the influence of process parameters on mechanical properties of fused deposition modeling parts. Micromachines 2022;13 (4). https://doi.org/10.3390/mi13040553.
[16] Pulipaka A, Gide KM, Beheshti A, Bagheri ZS. Effect of 3D printing process parameters on surface and mechanical properties of FFF-printed PEEK. J Manuf Process 2023;85:368–86. https://doi.org/10.1016/j.jmapro.2022.11.057.
[17] Yang C, Tian X, Li D, Cao Y, Zhao F, Shi C. Influence of thermal processing conditions in 3D printing on the crystallinity and mechanical properties of PEEK material. J Mater Process Technol 2017;248:1–7. https://doi.org/10.1016/j.jmatprotec.2017.04.027.

[18] Wang P, Zou B, Xiao H, Ding S, Huang C. Effects of printing parameters of fused deposition modeling on mechanical properties, surface quality, and microstructure of PEEK. J Mater Process Technol 2019;271:62–74. https://doi.org/10.1016/j.jmatprotec.2019.03.016.

[19] Rodzeń K, Harkin-Jones E, Wegrzyn M, Sharma PK, Zhigunov A. Improvement of the layer-layer adhesion in FFF 3D printed PEEK/carbon fibre composites. Compos Part A: Appl Sci Manuf 2021;149. https://doi.org/10.1016/j.compositesa.2021.106532.

[20] Massocchi D, Riboni G, Lecis N, Chatterton S, Pennacchi P. Tribological characterization of polyether ether ketone (PEEK) polymers produced by additive manufacturing for hydrodynamic bearing application. Lubricants 2021;9(11). https://doi.org/10.3390/lubricants9110112.

[21] Arif MF, Alhashmi H, Varadarajan KM, Koo JH, Hart AJ, Kumar S. Multifunctional performance of carbon nanotubes and graphene nanoplatelets reinforced PEEK composites enabled via FFF additive manufacturing. Compos Part B: Eng 2020;184. https://doi.org/10.1016/j.compositesb.2019.107625.

[22] Wang P, Zou B, Ding S, Zhuang Y, Liu J, Li L. Functionally graded polyetheretherketone-based composites additively manufactured by material extrusion using a transition interface design method. Compos Part A: Appl Sci Manuf 2022;158. https://doi.org/10.1016/j.compositesa.2022.106977.

[23] He Y, Shen M, Wang Q, Wang T, Pei X. Effects of FDM parameters and annealing on the mechanical and tribological properties of PEEK. Compos Struct 2023;313. https://doi.org/10.1016/j.compstruct.2023.116901.

[24] ASTM, *D792 - Standard Test Methods for Density and Specific Gravity (Relative Density) of Plastics by Displacement*. 2020. DOI: ⟨https://doi.org/10.1520/D0792–20⟩.

[25] ASTM, *D2734 - Standard Test Methods for Void Content of Reinforced Plastics*. 2016. DOI: ⟨https://doi.org/10.1520/D2734–16⟩.

[26] Blundell DJ, Osborn BN. The morphology of poly(aryl-ether-ether-ketone). Polymer 1983;24(8):953–8. https://doi.org/10.1016/0032-3861(83)90144-1.

[27] Gao S-L, Kim J-K. Cooling rate influences in carbon fibre-PEEK composites. Part 1. Crystallinity and interface adhesion. Compos: Part A 2000;31(6). https://doi.org/10.1016/S1359-835X(00)00009-9.

[28] ASTM, *D638 - Standard Test Method for Tensile Properties of Plastics*. 2014. DOI: https://doi.org/10.1520/d0638–14.

[29] Ren G., and Feng, J., *Friction and Wear Characteristics of ThorPlas Bearings and Their Application in Hydro Turbines*, in *Proceedings of the HydroVision International, Sacramento, CA USA*. 2011.

[30] Wasilczuk M. Friction and lubrication of large tilting-pad thrust bearings. Lubricants 2015;3(2):164–80. https://doi.org/10.3390/lubricants3020164.

[31] ASTM, *D570–22 Standard Test Method for Water Absorption of Plastics* . 2022. DOI: ⟨https://doi.org/10.1520/D0570–22⟩.

[32] Victrex. *Victrex_TDS_450G*. [cited June 2023; Available from: ⟨https://www.victrex.com/en/downloads/datasheets/victrex-peek-450g⟩.

[33] El Magri A, El Mabrouk K, Vaudreuil S, Chibane H, Touhami ME. Optimization of printing parameters for improvement of mechanical and thermal performances of 3D printed poly(ether ether ketone) parts. J Appl Polym Sci 2020;137(37). https://doi.org/10.1002/app.49087.

[34] Greenhalgh ES. Delamination-dominated failures in polymer composites. Failure Analysis and Fractography of Polymer Composites. Woodhead Publishing,; 2009. p. 164–237. https://doi.org/10.1533/9781845696818.164.

[35] Dhakal N, Wang X, Espejo C, Morina A, Emami N. Impact of processing defects on microstructure, surface quality, and tribological performance in 3D printed polymers. J Mater Res Technol 2023;23:1252–72. https://doi.org/10.1016/j.jmrt.2023.01.086.

[36] Stepashkin AA, Chukov DI, Senatov FS, Salimon AI, Korsunsky AM, Kaloshkin SD. 3D-printed PEEK-carbon fiber (CF) composites: Structure and thermal properties. Compos Sci Technol 2018;164:319–26. https://doi.org/10.1016/j.compscitech.2018.05.032.

[37] Unal H, Mimaroglu A. Friction and wear characteristics of PEEK and its composite under water lubrication. J Reinf Plast Compos 2006;25(16):1659–67. https://doi.org/10.1177/0731684406068406.

[38] Myshkin NK, Petrokovets MI, Kovalev AV. Tribology of polymers: adhesion, friction, wear, and mass-transfer. Tribology Int 2005;38(11-12):910–21. https://doi.org/10.1016/j.triboint.2005.07.016.

[39] Zhang G, Yu H, Zhang C, Liao H, Coddet C. Temperature dependence of the tribological mechanisms of amorphous PEEK (polyetheretherketone) under dry sliding conditions. Acta Mater 2008;56(10):2182–90. https://doi.org/10.1016/j.actamat.2008.01.018.

[40] Yamamoto Y, Takashima T. Friction and wear of water lubricated PEEK and PPS sliding contacts. Wear 2002;253(7):820–6. https://doi.org/10.1016/S0043-1648(02)00059-5.

[41] Laux KA, Schwartz CJ. Influence of linear reciprocating and multi-directional sliding on PEEK wear performance and transfer film formation. Wear 2013;301(1-2):727–34. https://doi.org/10.1016/j.wear.2012.12.004.

[42] Lin L, Pei X-Q, Bennewitz R, Schlarb AK. Friction and wear of PEEK in continuous sliding and unidirectional scratch tests. Tribology Int 2018;122:108–13. https://doi.org/10.1016/j.triboint.2018.02.035.

[43] Laux KA, Jean-Fulcrand A, Sue HJ, Bremner T, Wong JSS. The influence of surface properties on sliding contact temperature and friction for polyetheretherketone (PEEK). Polymer 2016;103:397–404. https://doi.org/10.1016/j.polymer.2016.09.064.

[44] Schroeder R, Torres FW, Binder C, Klein AN, de Mello JDB. Failure mode in sliding wear of PEEK based composites. Wear 2013;301(1-2):717–26. https://doi.org/10.1016/j.wear.2012.11.055.

[45] Voss H, Friedrich K. On the wear behaviour of short-fibre-reinforced PEEK composites. Wear 1987;116(1-18). https://doi.org/10.1016/0043-1648(87)90262-6.

[46] Greco AC, Erck R, Ajayi O, Fenske G. Effect of reinforcement morphology on high-speed sliding friction and wear of PEEK polymers. Wear 2011;271(9-10):2222–9. https://doi.org/10.1016/j.wear.2011.01.065.

[47] Zhang Z, Breidt C, Chang L, Friedrich K. Wear of PEEK composites related to their mechanical performances. Tribology Int 2004;37(3):271–7. https://doi.org/10.1016/j.triboint.2003.09.005.

[48] Avanzini A, Donzella G, Mazzù A, Petrogalli C. Wear and rolling contact fatigue of PEEK and PEEK composites. Tribology Int 2013;57:22–30. https://doi.org/10.1016/j.triboint.2012.07.007.

[49] Bahadur S. The development of transfer layers and their role in polymer tribology. Wear 2000;245(1-2):92–9. https://doi.org/10.1016/S0043-1648(00)00469-5.

[50] Jacobs O, Jaskulka R, Yan C, Wu W. On the effect of counterface material and aqueous environment on the sliding wear of various PEEK compounds. Tribology Lett 2005;18(3):359–72. https://doi.org/10.1007/s11249-004-2766-3.

[51] Golchin A, Simmons GF, Glavatskih S, Prakash B. Tribological behaviour of polymeric materials in water-lubricated contacts. Proc Inst Mech Eng, Part J: J Eng Tribology 2013;227(8):811–25. https://doi.org/10.1177/1350650113476441.

[52] Cole KC, Casella IG. Fourier transform infrared spectroscopic study of thermal degradation in films of poly(etheretherketone). Thermochim Acta 1992;211:209–28. https://doi.org/10.1016/0040-6031(92)87021-2.

[53] Puhan D, Wong JSS. Properties of Polyetheretherketone (PEEK) transferred materials in a PEEK-steel contact. Tribology Int 2019;135:189–99. https://doi.org/10.1016/j.triboint.2019.02.028.

[54] Pascual A, Toma M, Tsotra P, Grob MC. On the stability of PEEK for short processing cycles at high temperatures and oxygen-containing atmosphere. Polym Degrad Stab 2019;165:161–9. https://doi.org/10.1016/j.polymdegradstab.2019.04.025.

[55] Cole KC, Casella IG. Fourier transform infra-red spectroscopic study of thermal degradation in poly(ether ether ketone)-carbon composites. Polymer 1993;34(4):740–5. https://doi.org/10.1016/0032-3861(93)90357-G.

[56] Courvoisier E, Bicaba Y, Colin X. Multi-scale and multi-technique analysis of the thermal degradation of poly(ether ether ketone). Polym Degrad Stab 2018;151:65–79. https://doi.org/10.1016/j.polymdegradstab.2018.03.001.

[57] Gaitanelis D, Worrall C, Kazilas M. Detecting, characterising and assessing PEEK's and CF-PEEK's thermal degradation in rapid high-temperature processing. Polym Degrad Stab 2022;204. https://doi.org/10.1016/j.polymdegradstab.2022.110096.